stresses

MDPI

Article

In Vivo Anti-Inflammatory and Wound Healing Activity of Extracts and Micro-Aerogels of *Bursera microphylla* A. Gray

Juan Ramón Cañez-Orozco [1], Juan José Acevedo-Fernández [2], Julio César López-Romero [3], Victor Alonso Reyna-Urrutia [3], Ramón Enrique Robles-Zepeda [1,*] and Heriberto Torres-Moreno [3,*]

[1] Departamento de Ciencias Químico Biológicas, Universidad de Sonora, Boulevard Luis Encinas y Rosales s/n, Hermosillo 83600, Sonora, Mexico; a210218361@unison.mx
[2] Facultad de Medicina, Universidad Autónoma del Estado de Morelos, Calle Leñeros, Col. Volcanes, Cuernavaca 62350, Morelos, Mexico; juan.acevedo@uaem.mx
[3] Departamento de Ciencias Químico Biológicas y Agropecuarias, Universidad de Sonora, Avenida K SN, Caborca 83600, Sonora, Mexico; julio.lopez@unison.mx (J.C.L.-R.); alonso.reyna@unison.mx (V.A.R.-U.)
* Correspondence: robles.zepeda@unison.mx (R.E.R.-Z.); heriberto.torres@unison.mx (H.T.-M.)

Abstract: Chitosan micro-aerogels (CsM) are an innovative strategy for the controlled release of healing and anti-inflammatory ingredients. Although *Bursera microphylla* has anti-inflammatory activity in vitro, its in vivo effect is unknown. This study evaluated the anti-inflammatory and wound-healing effects of extracts and micro-aerogels of *B. microphylla*. Chitosan micro-aerogels loaded with 0.5% (CsMBT-0.5) and 1% (CsMBT-1) *B. microphylla* ethanol extract were characterized by SEM, FTIR, TGA, and moisture absorption. Cytotoxicity was assessed by MTT assay, and anti-inflammatory effects in vitro were evaluated by NO quantification. Anti-inflammatory and wound-healing effects in vivo were tested in CD1 mice. The microparticles measured 135–180 µm. FTIR showed that the extract's compounds remained unchanged during synthesis. TGA indicated degradation of the micro-aerogels between 250–350 °C and reduced moisture absorption when loaded with the extract. The extract inhibited NO release by 36% at 6.25 µg/mL and CsMBT-1 by 46% at 100 µg/mL ($p < 0.05$). The extract and CsMBT-0.5 in mice reduced ear swelling by 70% at 30 mg/mL ($p < 0.0001$). The extract reduced wound size by day 9, while CsMBT-0.5 accelerated wound closure from day 1 ($p < 0.05$), indicating that chitosan micro-aerogels were a promising anti-inflammatory and wound-healing treatment option.

Keywords: *Bursera microphylla*; chitosan micro-aerogels; anti-inflammatory effect; wound healing

Academic Editor: Nebojša Jasnić

Received: 16 November 2024
Revised: 28 December 2024
Accepted: 22 January 2025
Published: 27 January 2025

Citation: Cañez-Orozco, J.R.; Acevedo-Fernández, J.J.; López-Romero, J.C.; Reyna-Urrutia, V.A.; Robles-Zepeda, R.E.; Torres-Moreno, H. In Vivo Anti-Inflammatory and Wound Healing Activity of Extracts and Micro-Aerogels of *Bursera microphylla* A. Gray. *Stresses* **2025**, *5*, 10. https://doi.org/10.3390/stresses5010010

1. Introduction

Acute and chronic wounds represent a significant challenge for both affected individuals and healthcare systems worldwide [1]. The management of these wounds involves considerable financial investment due to the need for specialized personnel training, medical supplies, the management of increased infection rates, and the prolonged hospital stays that are often required. In addition to the high costs associated with these treatments, chronic wounds negatively impact patients, affecting them both physically and mentally [2–4]. This may lead to feelings of anxiety, depression, anger, frustration, loss of mobility, and decreased work capacity [5].

Cellular stress plays a crucial role in the pathogenesis of chronic wounds [6]. The persistence of an inflammatory microenvironment promotes the accumulation of reactive oxygen species (ROS) and other stress signals, such as the activation of pro-inflammatory signaling pathways like the NF-κB pathway and increased pro-inflammatory cytokines

(IL-1β, IL-6, and TNF-α), which can lead to cellular dysfunction and perpetuate the inflammatory state [7]. This situation not only compromises the cells' ability to repair damaged tissue but also disrupts cellular homeostasis, exacerbating the chronicity of the wound [8]. When cellular mechanisms fail to resolve an acute wound adequately, it can evolve into a chronic wound, interrupting or delaying the normal healing process [9,10]. Various risk factors, such as diabetes, vascular diseases, autoimmune disorders, cancer, obesity, and malnutrition, can aggravate cellular stress and further hinder healing [11–13], therefore, restoring tissue integrity, adequately managing cellular stress, and maintaining homeostasis are fundamental aspects of wound treatment [14].

Managing cellular stress and restoring homeostasis is crucial for effective wound healing [15,16]. Among the most commonly used drugs for this purpose are non-steroidal anti-inflammatory drugs (NSAIDs) and topical wound-healing agents [17–19]. Although these medications are effective in reducing inflammation and promoting healing, they are also associated with significant side effects, such as gastrointestinal issues, bleeding risk, kidney failure, heart problems, allergic reactions, delayed healing, and skin irritation [20,21].

In this context, semi-solid formulations have been recognized as a promising option for the treatment of skin conditions, offering multiple advantages such as excellent absorption, low irritability, and microadhesive properties [22]. The use of polysaccharides for the preparation of hydrogels has gained popularity in recent years due to their outstanding biocompatibility and biodegradability properties, making them an ideal option for wound healing [23,24]. Within this category, chitosan (CS) is a versatile polysaccharide widely studied for its hemostatic, antibacterial, anti-inflammatory, and wound-healing effects. In addition, chitosan offers controlled release capabilities and the ability to form three-dimensional matrices, making it particularly valuable in advanced medical applications [25–27]. A recent innovation in this field is the development of chitosan aerogels, which can also be produced in micrometric sizes as micro-aerogels. These three-dimensional systems are obtained through a physical cross-linking process using ammonium hydroxide followed by lyophilization [28]. This process creates a porous, interconnected matrix structure by removing ice crystals from the frozen CS solution [29]. In addition, the clinical relevance of chitosan micro-aerogels lies in their potential to address multiple challenges in wound treatment, particularly in patients with chronic or complicated conditions that require special attention. By integrating the effects of CS with the benefits of plant extracts that possess anti-inflammatory and wound-healing properties, their therapeutic efficacy could be significantly enhanced [30,31]. The use of plants with wound-healing properties has been widely reported. These plants often exhibit anti-inflammatory, antimicrobial, and antioxidant effects, which are important to promote tissue regeneration and accelerate the healing process. Many plant-based extracts have shown promising results, making them valuable in therapeutic applications for wound care [32–34].

Bursera microphylla A. Gray (Burseraceae) is a plant widely distributed in the desert region of northern Mexico and the southwestern United States. In traditional Mexican medicine, the Seri ethnic group uses its bark, leaves, flowers, and fruits to treat sore throats and headaches and promote wound healing [35]. Recently, the identification of various diterpenoids, triterpenoids, lignans, and phenolic compounds with cytotoxic, antiproliferative, and antioxidant activities from extracts and fractions of *B. microphylla* has been reported [36]. It is also known that seasonality modulates the anti-inflammatory and antiproliferative effects of the fruits, leaves, and stems of *B. microphylla* [37]. This anti-inflammatory effect has been associated with lignan-type compounds, such as burseran, β-peltatin A-methyl ether, ariensin, and dihydroclusin diacetate [38]. *B. microphylla* stems have shown anti-inflammatory activity in nitric oxide (NO) and TNF-α reduction assays. Although the anti-inflammatory properties of *B. microphylla* have not been evaluated in vivo, and its wound-healing potential remains unexplored, it is noteworthy that, to date,

no formulation incorporating extracts or bioactive compounds derived from this plant has been developed. This study aims to investigate the anti-inflammatory and wound-healing activities of ethanolic extracts of *B. microphylla* and CsM loaded with these extracts, expanding knowledge about the therapeutic potential of *B. microphylla* and enhancing our understanding of chitosan-based delivery systems.

2. Results

2.1. Physicochemical Characterization of Chitosan Micro-Aerogels

2.1.1. SEM Characterization of Micro-Aerogels

To analyze the size and morphology of the micro-aerogels (CsM, CsMBT-0.5, CsMBT-1), optical microscopy (OM) and scanning electron microscopy (SEM) were employed. While OM provides an overview of the microparticle morphology and particle size, SEM offers detailed information regarding the structure and distribution of the *B. microphylla* extract within the chitosan microparticles, allowing for a better understanding of their physical properties and potential applications. Figure 1 shows the SEM micrographs of chitosan microparticles loaded with *B. microphylla* extract, providing detailed insights into the structure and distribution of the extract within the system. SEM analysis of the chitosan micro-aerogel (CsM) revealed a laminar structure with significant porosity. This laminar feature is crucial for its potential applications, as it increases surface area and interaction with biological environments (Figure 1A). The porosity enhances fluid retention and contributes to the controlled diffusion of active compounds, which is particularly important in pharmaceutical and biomedical applications. Additionally, the porous design of the micro-aerogel creates an optimal environment for cell growth, which is essential for tissue engineering and regenerative medicine applications [39].

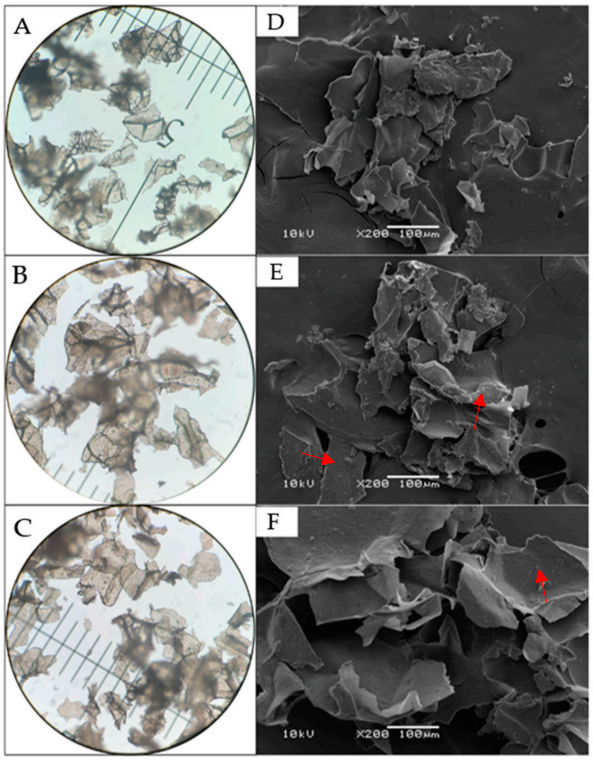

Figure 1. Optical microscopy (OM) and scanning electron microscopy (SEM) of micro-aerogels at 200×. (**A**) OM of chitosan micro-aerogel (CsM). (**B**) OM of 1% loaded micro-aerogel (CsMBT-1). (**C**) OM of 0.5% loaded micro-aerogel (CsMBT-0.5). (**D**) SEM of chitosan micro-aerogel (CsM). (**E**) SEM of 1% loaded micro-aerogel (CsMBT-1). (**F**) SEM of 0.5% loaded micro-aerogel (CsMBT-0.5). Red arrows indicate *B. microphylla* extract present in the microparticles.

By incorporating the *B. microphylla* extract (0.5%) into the formulation (CsMBT-0.5), the micrographs revealed the presence of small, round bodies distributed homogeneously throughout the micro-aerogel matrix (Figure 1E). This observation suggests an effective incorporation of the extract within the chitosan polymer walls that form the three-dimensional network of the micro-aerogel, indicating a successful encapsulation of the active components. This encapsulation suggests that the preparation method allows for a homogeneous distribution of the extract within the chitosan matrix, which is crucial for ensuring the controlled and sustained release of the extract in biomedical applications. Moreover, effective encapsulation can protect the bioactive components of the extract, maintaining their functionality and stability during storage and use [40–42].

A higher frequency of rounded bodies was observed in the samples loaded with 1.0% *B. microphylla* extract (CsMBT-1), suggesting a direct relationship between the concentration of the extract and the formation of these structures (Figure 1F). These rounded bodies may represent agglomerates of encapsulated extract, indicating that at higher concentrations, the extract tends to form larger clusters within the hydrogel matrix. This phenomenon could influence the size of the microparticles of the micro-aerogel and contribute to the mechanical and functional properties of the material, such as porosity and the release of bioactive substances [29,43].

2.1.2. Size Frequency of Micro-Aerogels

The knowledge of microparticle size is essential for understanding how these variations can influence the physical and functional properties of micro-aerogels, which, in turn, affects their performance in biomedical and pharmaceutical applications [44]. The results reveal that micro-aerogels exhibit variations in their sizes that are associated with the concentration of the extract used in the synthesis. Firstly, for CsM (unloaded micro-aerogel), it was observed that the size frequency of the micro-aerogel is primarily concentrated at 135 µm, with a bimodal distribution skewed to the right. However, with an increase in the concentration of *B. microphylla* extract, there is a noticeable increase in the average size, which may be due to the formation of agglomerates of the extract within the chitosan matrix, influencing the dynamics of microparticle formation. This behavior suggests that the presence of the extract affects the distribution and encapsulation within the chitosan matrix and modifies the morphological properties of the micro-aerogels [45]. In the loaded micro-aerogels CsMBT-0.5 and CsMBT-1, changes in the size distribution were observed compared to CsM, with an unimodal distribution skewed to the right. In CsMBT-0.5, a frequency of 135 µm size was recorded, and a second size frequency of 180 µm was observed, showing a trend of an unimodal distribution skewed to the left. This phenomenon confirms that the incorporation of the extract into the chitosan matrix influences the formation of larger microparticle sizes. On the other hand, increasing the extract concentration to 1.0% resulted in a significant change in the microparticle size distribution. In this case, the highest frequency was recorded at 180 µm, reaffirming that a higher concentration of extract may promote the formation of larger microparticle sizes (Figure 2). This result may be crucial for understanding how extract concentration can modulate the physical properties of micro-aerogels, which could, in turn, affect their performance in specific applications, such as the controlled release of bioactive compounds [46].

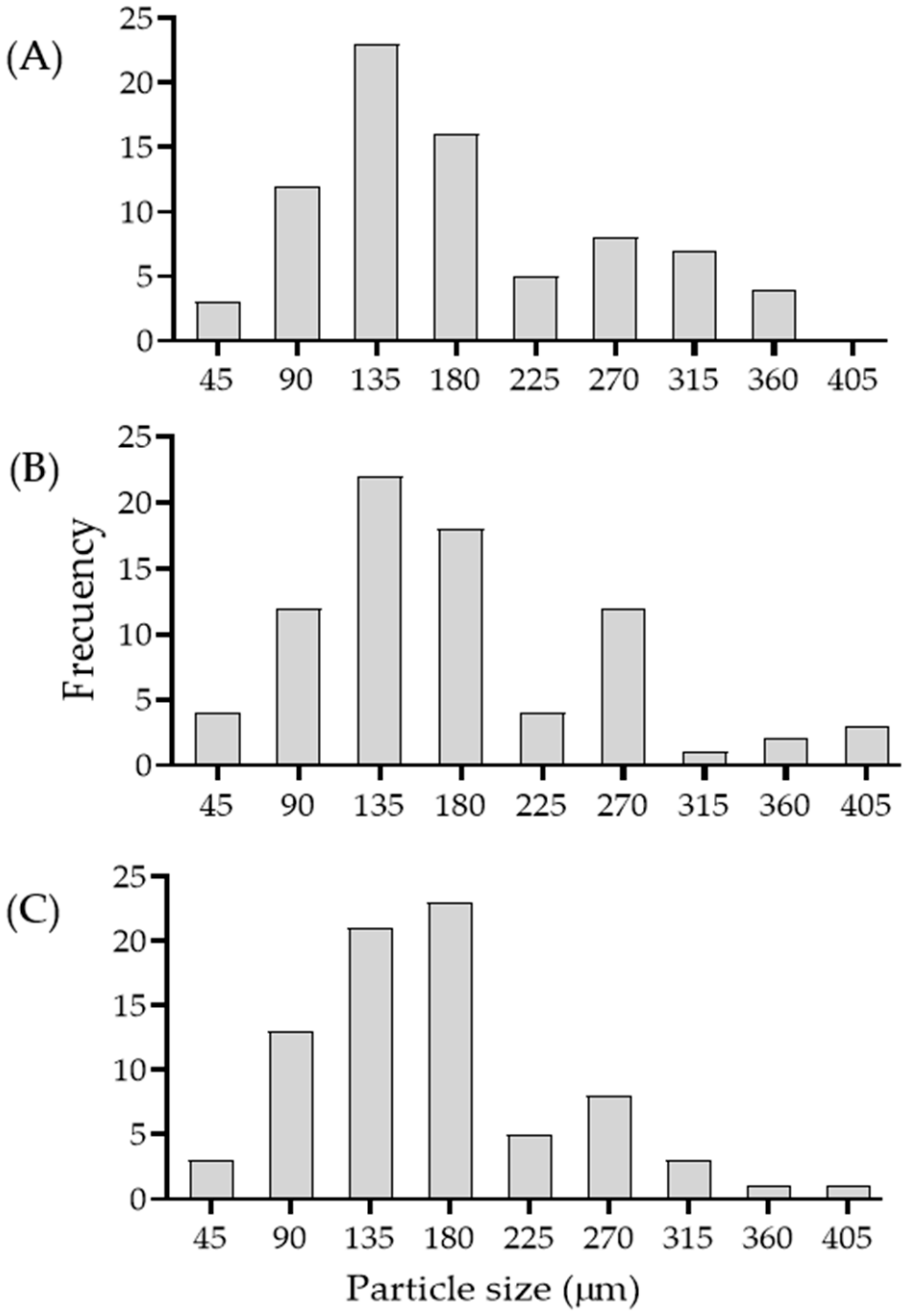

Figure 2. Size distribution of micro-aerogels obtained by freeze-drying from hydrogels. (**A**) Chitosan Micro-aerogel (CsM). (**B**) 1% Loaded Micro-aerogel (CsMBT-1). (**C**) 0.5% Loaded Micro-aerogel (CsMBT-0.5).

2.1.3. FTIR Analysis

FTIR analysis is crucial for identifying the functional groups and molecular interactions present in the micro-aerogels, allowing us to understand the bonds formed between chitosan and the *B. microphylla* extract (Figure 3). The FTIR results highlight the presence of functional groups responsible for their unique properties. The broadband in the 3500–3300 cm^{-1} range, corresponding to the O–H and N–H stretching vibrations, indicates the presence of hydroxyl and amine groups. The peaks at 2923 and 2880 cm^{-1} suggest the presence of methyl groups.

The bands observed at 1653 cm^{-1} (amide I) and 1580 cm^{-1} (amide II) confirm the presence of amide structures in chitosan derived from the deacetylation of chitin. The signals recorded in the range of 1200–1000 cm^{-1} are associated with the saccharide structure. A peak observed in the range of 1710–1730 cm^{-1}, which is absent in chitosan (Cs), may be related to carbonyl stretching vibrations (C=O). This suggests the presence of aldehyde

and ketone groups, which could be interacting with the chitosan matrix. The comparative analysis of the FTIR signals reveals that the unloaded and loaded microparticles with extract exhibit similar signal patterns, indicating no new functional groups in the loaded microparticles. This confirms the absence of chemical interactions between Cs and the *B. microphylla* extract, suggesting that the compounds in the extract do not undergo chemical changes during the microparticle synthesis process and that the activity of the extract remains unaffected [47–50].

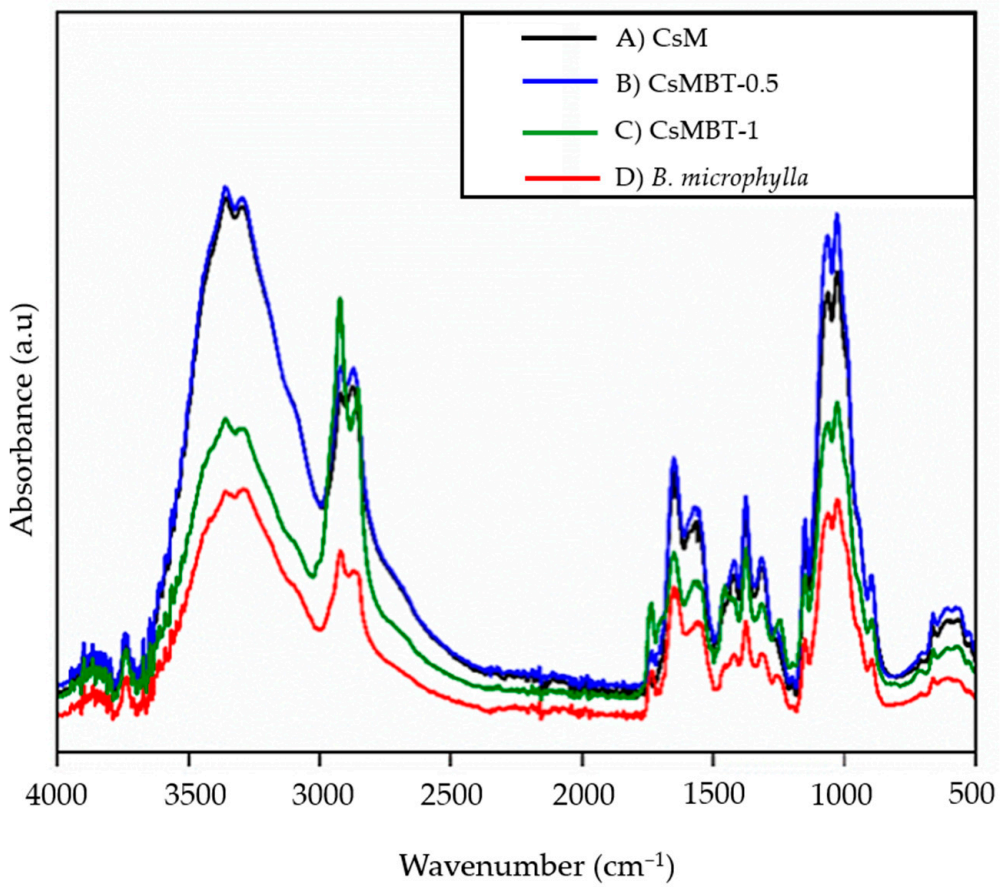

Figure 3. Fourier Transform Infrared Spectroscopy (FTIR) Analysis of chitosan micro-aerogels. (A) Chitosan micro-aerogel (CsM). (B) Micro-aerogel loaded at 1% (CsMBT-1). (C) Micro-aerogel loaded at 0.5% (CsMBT-0.5). (D) Ethanolic extract of *B. microphylla* stems.

2.1.4. Moisture Absorption Analysis of Micro-Aerogels

After analyzing the chemical structure and molecular interactions of chitosan micro-aerogels using FTIR spectroscopy, it is essential to investigate how these properties influence their ability to absorb and retain moisture, which is particularly relevant for assessing their viability in biotechnological applications, such as wound healing.

Under 80 ± 1% humidity conditions, the CsM showed a greater capacity for moisture absorption compared to the CsMBT-0.5 and CsMBT-1. Similarly, at 40 ± 1% humidity, CsM outperformed CsMBT-0.5 and CsMBT-1 in moisture absorption and in a shorter time. These differences in moisture absorption suggest significant implications for the performance of the micro-aerogels. The higher moisture absorption capacity of CsM may pose challenges regarding its chemical and physical stability over time, potentially limiting its efficacy in high-humidity environments. Conversely, the lower moisture absorption observed in CsMBT-0.5 and CsMBT-1 could enhance its stability and prolong its shelf life [51]. Additionally, moisture stability or saturation was observed around days 18 to

19 of this analysis, providing valuable insights into the behavior of these materials under prolonged storage conditions. (Figure 4) [52].

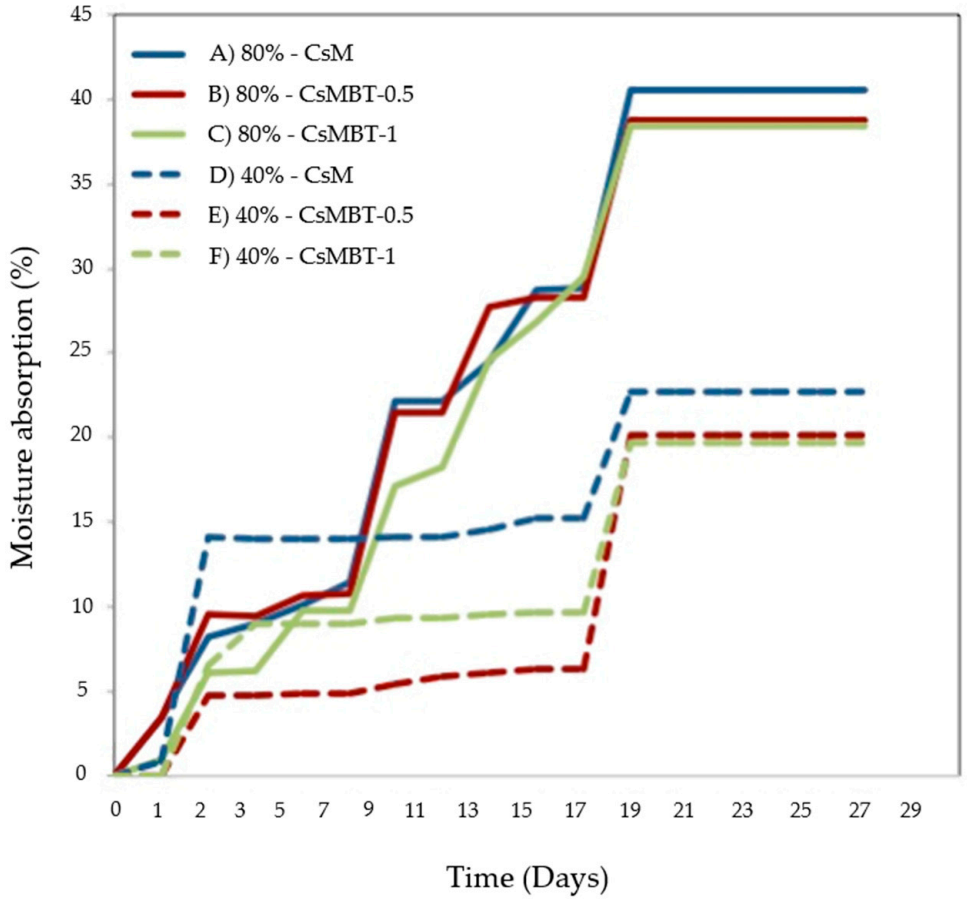

Figure 4. Moisture absorption analysis of micro-aerogels. (A) Chitosan micro-aerogel (CsM) at 80% humidity. (B) Micro-aerogel loaded at 0.5% (CsMBT-0.5) at 80% humidity. (C) Micro-aerogel loaded at 1% (CsMBT-0.5) at 80% humidity. (D) Chitosan micro-aerogel (CsM) at 40% humidity. (E) Micro-aerogel loaded at 0.5% (CsMBT-1) at 40% humidity. (F) Micro-aerogel loaded at 1% (CsMBT-0.5) at 40% humidity.

2.1.5. Thermogravimetric Analysis (TGA)

Thermogravimetric analysis (TGA) is a crucial technique for understanding the thermal stability and degradation of polymeric materials, such as micro-aerogels, and the components that make up the polymeric matrix of the micro-aerogels. Lyophilization allows for the controlled removal of solvent, resulting in a highly interconnected porous structure that preserves the integrity of active components, such as the extract from *B. microphylla*, suggesting that the lyophilization process maintains the bioactivity of these compounds during the micro-aerogel formation [53,54]. The TGA analysis provides valuable insights into the thermal stability of the extract and the microparticles. The extract showed a mass loss of ≈80% between 50–100 °C, with a maximum peak observed at 78 °C (see green arrow), indicating its low thermal stability and high sensitivity to heat. In contrast, the microparticles (CsM, CsMBT-0.5, CsMBT-1.0) experienced a smaller mass loss of ≈5% at ≈100 °C, attributed to the loss of water molecules. A second mass loss for the microparticles occurred at approximately 300 °C (see red arrow), corresponding to the degradation of saccharides in the chitosan molecule. This behavior aligns with the previously observed decomposition range of 250 to 350 °C for the polymeric and biological components of the micro-aerogels. Among the tested formulations, the CsMBT-0.5 micro-aerogel exhibited

superior thermal stability, showing a weight loss of only 52–56% at 600 °C (see blue arrow), further highlighting its resilience under high-temperature conditions (Figure 5) [55].

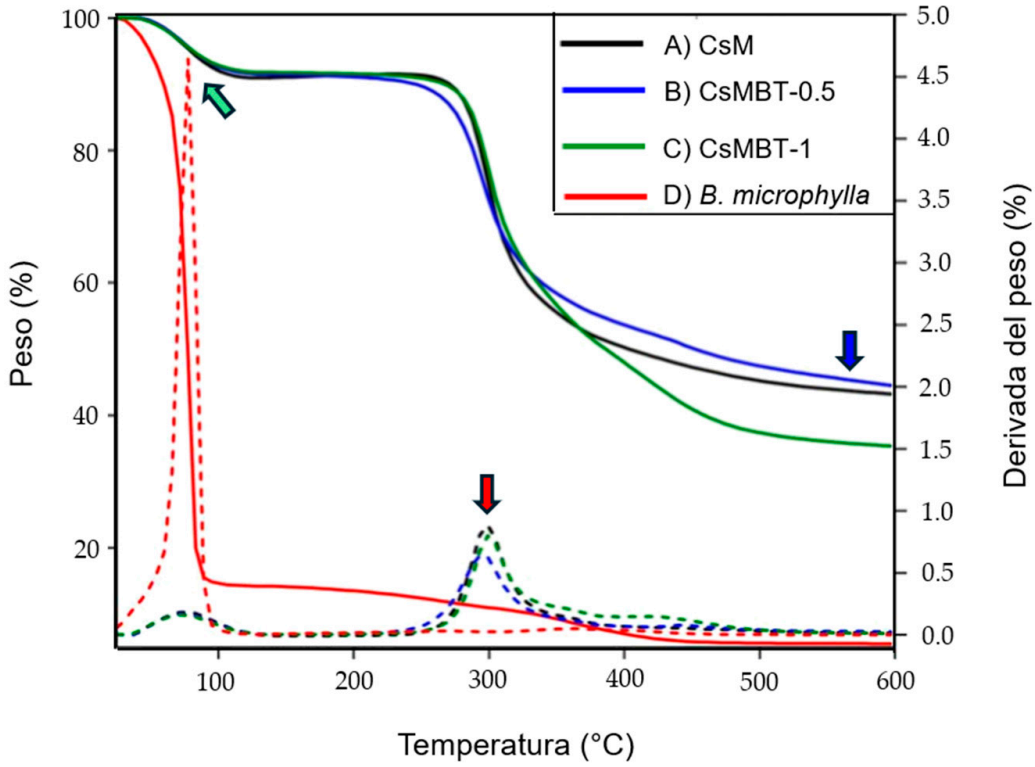

Figure 5. Thermogravimetric analysis (TGA) of the ethanolic extract of *B. microphylla* stems and the micro-aerogels. (A) Chitosan micro-aerogel (CsM). (B) Micro-aerogel loaded at 1% (CsMBT-1). (C) Micro-aerogel loaded at 0.5% (CsMBT-0.5). (D) Ethanolic extract of *B. microphylla* stems. Green arrow: Maximum loss of *B. microphylla* extract; Red arrow: Maximum loss of Cs and Cs with *B. microphylla* extract. Blue arrow: Weight loss of CsMBT-0.5. Dashed lines represent the derivative of the mass loss of the treatments.

2.2. Cytotoxic Effect

Before evaluating the effects of extracts or compounds on NO production in cellular models, it is essential to establish the non-cytotoxic concentrations using the MTT assay, which measures cell viability through mitochondrial activity. This ensures that observed effects are due to anti-inflammatory properties rather than cell death or stress responses [56].

At concentrations of 0.78 to 1.56 µg/mL of *B. microphylla* extract, cell viability remained above 90%, indicating minimal cytotoxic effects. However, at higher concentrations (3.12 and 6.25 µg/mL), viability dropped below 90%, likely due to the increased cytotoxicity of secondary metabolites that may disrupt cellular processes [57].

CsM at concentrations of 12.5 to 100 µg/mL showed cell viability from 100% to 88%, indicating lower cytotoxicity compared to the *B. microphylla* extract. In the case of CsMBT-0.5, cell viability decreased from 97% at 25 µg/mL to 79% at 100 µg/mL. Additionally, CsMBT-1 at concentrations of 25 to 100 µg/mL further reduced cell viability from 88.9% to 77.4%, demonstrating a further decrease in viability as the proportion of the extract in the formulation increased (Figure 6).

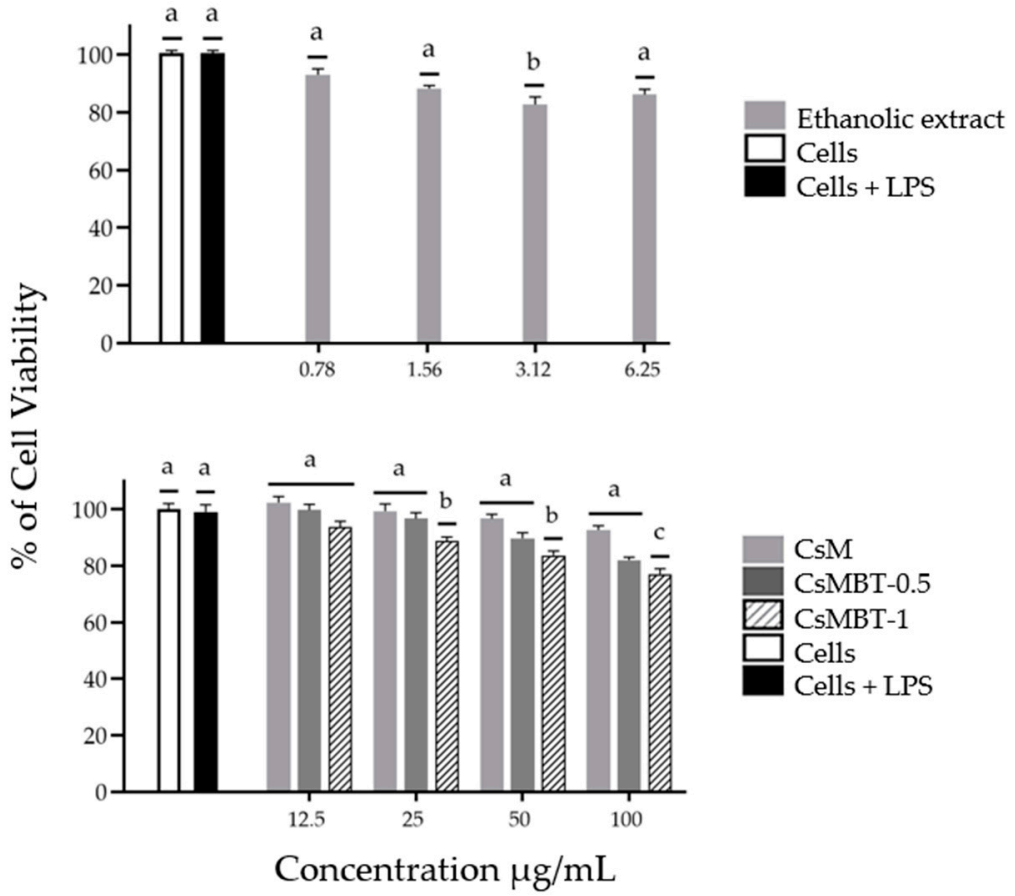

Figure 6. Effect of ethanolic extract and micro-aerogels of *B. microphylla* on the cell viability of RAW 264.7 macrophages. Bars with different superscripts indicate statistical differences ($p < 0.05$). All values represent three independent experiments' mean ± standard deviations (±SD, $n = 3$). Chitosan micro-aerogel (CsM). Chitosan micro-aerogel loaded at 1% (CsMBT-1). Chitosan micro-aerogel loaded at 0.5% (CsMBT-0.5). LPS (lipopolysaccharide).

2.3. Effect on NO Production of Bursera microphylla Extract

To evaluate the effect of the ethanolic extract of *B. microphylla* on NO production, concentrations ranging from 0.78 to 6.25 µg/mL were tested. Exposure of macrophages to LPS increases NO production compared to the basal level detected in untreated cells. After 24 h of treatment and stimulation, the *B. microphylla* extract reduced NO production by 22% and 25% at concentrations of 3.12 and 6.25 µg/mL, respectively, compared to the control (Cells + LPS).

Additionally, CsM demonstrated a NO reduction capacity of 28% and 39% at concentrations of 12.5 and 100 µg/mL. Meanwhile, CsMBT-0.5 reduced NO production by up to 40% at a concentration of 100 µg/mL. Notably, the micro-aerogel loaded with 1% extract (CsMBT-1) achieved a 46.1% reduction in NO production at the highest concentration of 100 µg/mL compared to the activation control ($p < 0.05$), showing better effect than CsM and CsMBT-0.5 at the same concentration ($p < 0.05$). (Figure 7).

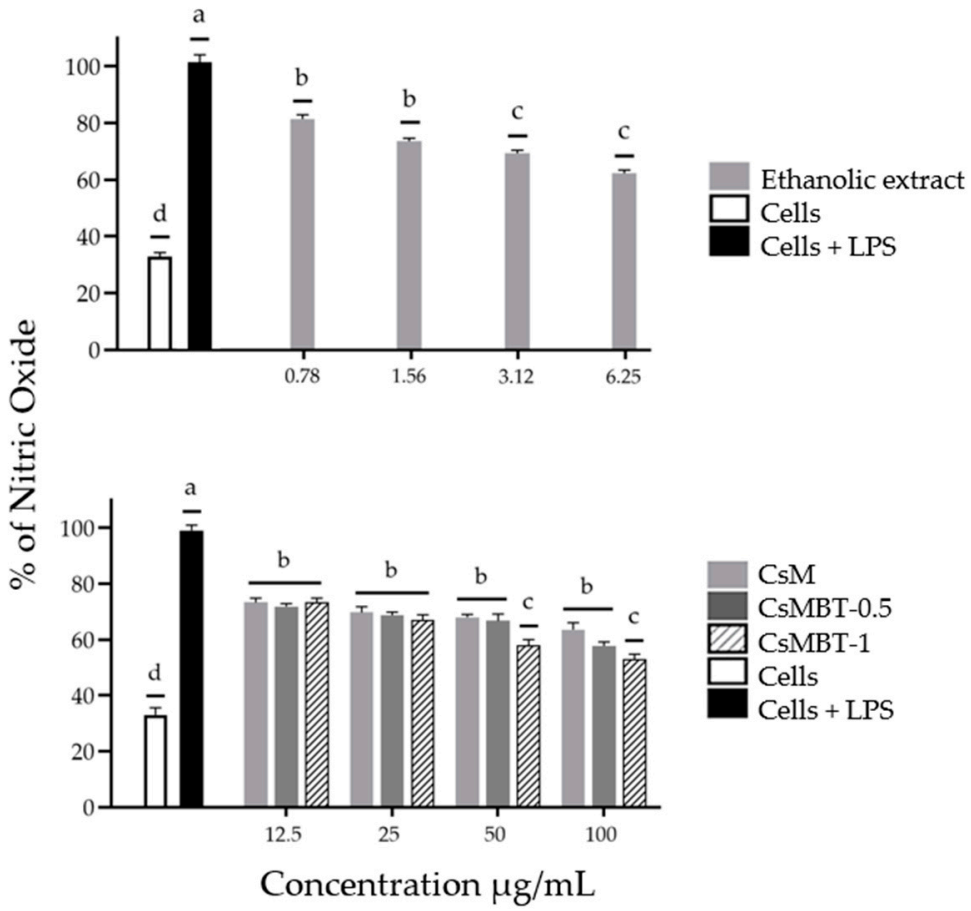

Figure 7. Effect of ethanolic extract and micro-aerogels of *B. microphylla* on the cell viability of RAW 264.7 macrophages. Bars with different superscripts indicate statistically significant differences ($p < 0.05$). All values represent three independent experiments' mean ± standard deviation (±SD, $n = 3$). Chitosan micro-aerogel (CsM). Chitosan micro-aerogel loaded at 1% with *B. microphylla* extract (CsMBT-1). 0.5% loaded micro-aerogel (CsMBT-0.5). LPS (lipopolysaccharide).

2.4. Anti-Inflammatory Effect on TPA-Induced Ear Edema

The anti-inflammatory effects of the ethanolic extract of *B. microphylla* stems and the micro-aerogels (CsM, CsMBT-0.5, and CsMBT-1) were evaluated in vivo using the TPA-induced ear edema model. In the group treated solely with TPA, which served as the inflammation activation control, an increase in ear thickness was observed, indicating inflammation. In contrast, the anti-inflammatory control (indomethacin at 30 mg/mL) demonstrated a 72.7% reduction in ear inflammation compared to the TPA group. CsM at 30 mg/mL exhibited a 40% reduction in inflammation, suggesting that chitosan alone may possess anti-inflammatory properties, potentially through interactions with immune cells or inflammatory mediators. The formulations of CsMBT, containing 0.5% (CsMBT-0.5) and 1% (CsMBT-1) extract, showed reductions in inflammation of 70.7% and 67%, respectively. This finding indicates that the combination of chitosan with a *B. microphylla* extract significantly enhances anti-inflammatory activity compared to CsM alone. Furthermore, the anti-inflammatory effect of the *B. microphylla* extract reduced inflammation by 70.7%, similar to the effect observed with the CsMBT-0.5 formulation, highlighting the potential of the extract in modulating inflammation in the TPA model (Figure 8).

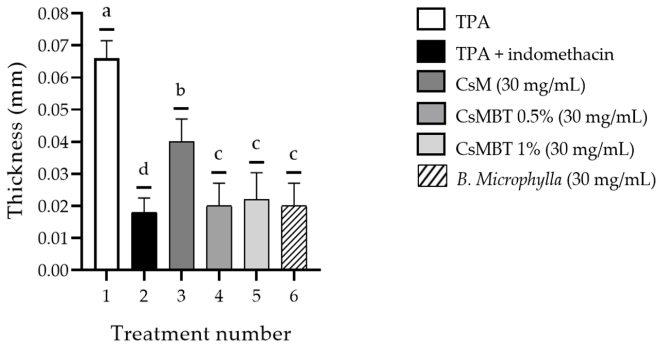

Figure 8. Evaluation of the anti-inflammatory effect of micro-aerogels and *B. microphylla* extract in the TPA-induced ear edema model. Treatments: (1) TPA (2) TPA + indomethacin 30 mg/mL. (3) CsM 30 mg/mL. (4) CsMBT-1 30 mg/mL. (5) CsMBT-1 30 mg/mL. (6) *B. microphylla*. $n = 5 \pm$ SEM. Bars with different superscripts indicate statistical differences ($p < 0.0001$). All values represent three independent experiments' mean ± standard deviation (±SD, $n = 3$).

2.5. Healing Effect

To evaluate the wound healing effect of the ethanolic extract of *B. microphylla* stems and micro-aerogels, a skin wound model was used in CD1 female mice. Wounds measuring 6 mm in diameter were created on the backs of the animals, and the healing process was observed for 12 days. The percentage of wound closure was then calculated, allowing for the assessment of area reduction compared to the initial size.

In the control group treated with SSF 0.9%, a 36% reduction in wound size was observed on the first day. The commercial wound healing agent KitosCell-Q achieved a 41% reduction in wound size on the first day. CsM reduced wound size by 48%, while CsMBT-0.5 and CsMBT-1 achieved a 62% and 54% reduction on the first day ($p < 0.001$), respectively. Furthermore, *B. microphylla* extract reduced wound size by 45%, showing a better effect than the control. On the sixth day after the treatment, SSF reduced wound size by 79%, KitosCell-Q by 82%, and CsM by 80%. CsMBT-0.5 showed the highest healing activity, closing 91% of the wound ($p < 0.001$). CsMBT-1, containing 1% extract, achieved an 84% reduction, comparable to the effect of the extract alone. *B. microphylla* extract demonstrated notable healing activity by day 9, achieving 99% closure, like the effect of CsMBT-0.5 ($p < 0.001$; Figure 9). The wound healing effects are qualitatively assessed in Figure 10, providing a visual comparison of the treatments and illustrating the progression of wound closure over time.

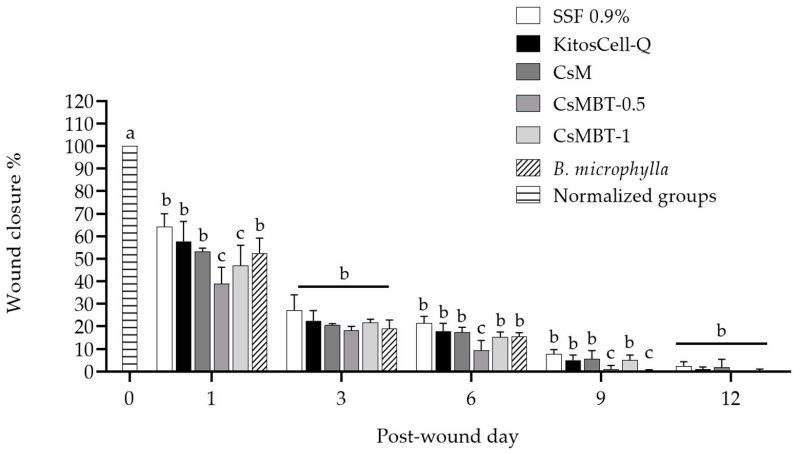

Figure 9. Wound healing effect in mice of micro-aerogels and *B. microphylla* extract. [a–c] Bars with different superscripts indicate statistical differences ($p < 0.0001$) of each treatment for each post-wound day. All values represent three independent experiments' mean ± standard deviation (±SD, $n = 3$). KitosCell-Q and the 9% physiological saline solution (SSF) were used as positive and vehicle controls.

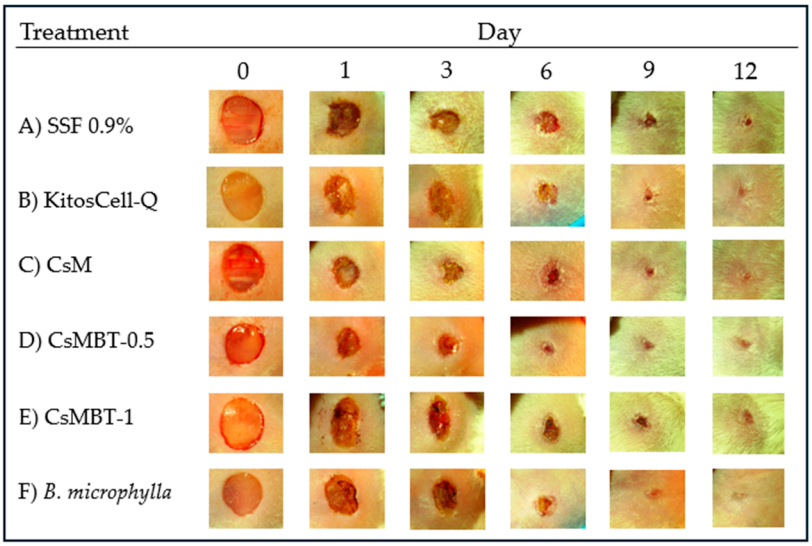

Figure 10. Photographs of the kinetics of lesions subjected to different treatments for 12 days. (A) A 9% physiological saline solution (SSF at 0.9%) (B) KitosCell-Q (C) Chitosan micro-aerogel (CsM) (D) Chitosan micro-aerogel with 0.5% *B. microphylla* (CsMBT-0.5) (E) Chitosan micro-aerogel with 1% *B. microphylla* (CsMBT-1) (F) *B. microphylla* extract at 30 mg/mL.

3. Discussion

Inflammation is a critical phase in the wound healing process, as it triggers the removal of pathogens and damaged tissue, preparing the environment for tissue repair [58]. However, excessive or prolonged inflammation can lead to poor wound healing, characterized by abnormal scarring or delayed healing [59]. In this context, modulating the inflammatory response becomes a key therapeutic target for improving healing outcomes [60]. In addition to inflammation, cellular stress is another relevant factor that arises under adverse conditions, such as the presence of free radicals, imbalances in proinflammatory signals, accumulation of toxic products, or mitochondrial dysfunction [61]. These elements not only exacerbate inflammation but also disrupt cellular function and impair tissue repair [62].

The physicochemical characterization of the micro-aerogels suggests that increasing the extract concentration in chitosan micro-aerogels results in larger microparticles, which could favor a controlled release of bioactive compounds. The FTIR spectra suggest that the extract compounds are stable within the CS matrix since no significant shifts or new peaks were observed. Furthermore, the absence of new signals suggests that there are no strong chemical interactions between CS and the *B. microphylla* extract. The characteristic peaks of CS, such as the amide I band (1653 cm^{-1}) and amide II band (1580 cm^{-1}), were retained in all formulations, confirming that the CS structure remains intact. Moreover, the peaks associated with the *B. microphylla* extract, including the carbonyl groups (around 1710–1730 cm^{-1}) and hydroxyl groups (3500–3300 cm^{-1}), were preserved, suggesting that the encapsulation process did not significantly alter the functional groups of the extract. Specifically, a peak in the range of 1710–1730 cm^{-1}, which is absent in CS, indicates the presence of carbonyl stretching vibrations (C=O), likely related to aldehyde or ketone groups in the extract. This suggests that, while there may be weak interactions, the encapsulation process preserves the extract's bioactivity without inducing significant chemical changes. These findings indicate that the encapsulation process did not interfere with the chemical integrity of the extract, which remains stable within the chitosan matrix. The reduction in moisture absorption observed in extract-loaded micro-aerogels suggests greater stability under storage conditions and humid environments, which would be important for wound applications. This phenomenon could be attributed to changes in the material's

hydrophobicity or porosity due to the encapsulation of *B. microphylla* extract, making it less hydrophilic. Further studies on the interaction between the extract and the polymeric matrix, as well as the structural characteristics of the micro-aerogels, would be needed to better understand the mechanisms behind these changes in moisture absorption. The TGA analysis complements these findings by indicating enhanced thermal stability in extract-loaded micro-aerogels. The extract itself exhibited low thermal stability, with significant degradation between 50 °C and 100 °C. However, encapsulation within the chitosan matrix conferred protection, as evidenced by the lower mass loss (≈5% at 100 °C) due to water evaporation and the delayed degradation onset (around 300 °C) of the saccharides in the polymer. Among the formulations, CsMBT-0.5 demonstrated superior thermal stability, with minimal weight loss (52–56%) at 600 °C [63]. Encapsulation within the polymeric matrix appears to create a protective environment for the extract's compounds, preserving their bioactivity and enhancing their thermal resistance [64]. The observed thermal stability of the micro-aerogels aligns with findings from studies on micro-aerogels loaded with medicinal plant extracts, where variations in degradation behaviors are attributed to the chemical composition of the extracts and the preparation and lyophilization processes. This reinforces the potential of incorporating *B. microphylla* extract into chitosan-based systems, not only for enhanced thermal stability but also for achieving effective therapeutic performance in wound-healing applications [65].

The cytotoxicity analysis revealed that the ethanolic extract of *B. microphylla* reduces cell viability. However, when the extract was encapsulated in chitosan micro-aerogels, cytotoxicity was reduced. This suggests that the micro-aerogel system acts as a protective vehicle, modulating the release of metabolites and reducing their cytotoxic effects. Moreover, the micro-aerogels' ability to maintain a suitable environment for cells further facilitates these processes. This suggests that encapsulating the extract in the CS matrix could enhance its application in wound healing models, highlighting the potential of CS-based micro-aerogels for the delivery of natural extracts [66].

Nitric oxide (NO) is a key proinflammatory mediator generated by macrophages in response to inflammatory stimuli such as LPS. Through toll-like receptor 4 (TLR4), macrophages recognize LPS, triggering an intracellular signaling cascade that results in the production of proinflammatory mediators and cytokines such as NO, TNF-α, IL-6, and IL-1β. Therefore, reducing the overproduction of NO is crucial in controlling inflammation [67]. The results suggest that CsM, CsMBT, and *B. microphylla* extract may influence some proteins involved in these signaling pathways, such as inducible nitric oxide synthase (iNOS), nuclear factor kappa B (NF-κB), and mitogen-activated protein kinases (MAPKs), which are critical in the modulation of the inflammatory response. Furthermore, the inclusion of *B. microphylla* extract in the micro-aerogels could enhance these effects, as the bioactive compounds present in the extract may interact with chitosan, potentially improving its anti-inflammatory efficacy (see Figure 7). This combined approach may help reduce NO and modulate other proinflammatory mediators, leading to a more comprehensive and sustained effect [68]. Regarding the cell viability results, it is important to emphasize that although NO reduction was observed at higher concentrations, cytotoxicity may influence this effect. However, the reduction in NO at concentrations where cell viability remains above 90% suggests that the decrease in NO is largely a pharmacological effect rather than solely a consequence of cellular damage. Thus, the observed effects on NO reflect both the anti-inflammatory capability of the extract and micro-aerogels, as well as a possible modulation of inflammatory signaling pathways beyond cytotoxicity at higher concentrations. In a previous study, CsM micro-aerogels loaded with *Bursera microphylla* fruit extract were evaluated, showing similar effects in the reduction in NO by approximately 40%, consistent with the findings in our study. Both approaches, the fruit extract and the micro-aerogels,

demonstrated significant anti-inflammatory activity, highlighting their ability to reduce NO production in LPS-activated RAW 264.7 cells. This suggests that *B. microphylla*-based formulations from the stem and fruit exhibit comparable anti-inflammatory effects [69,70].

The anti-inflammatory activity of *B. microphylla* extract in the TPA-induced ear edema model could be attributed to lignan compounds such as Hinokinin, Burseran, Ariensin, Dihydroclusin diacetate, and 7′, 8′-dehydropodophyllotoxin, which are present in the stem of *B. microphylla*. Given the structural similarities between these lignans and Hinokinin, their anti-inflammatory effects may be related to similar mechanisms of action, possibly involving modulation of inflammatory pathways associated with these compounds. The anti-inflammatory activity of Hinokinin has been documented, as it modulates oxidative stress and inflammation through the Nrf2/Keap/ARE and MAPK (JNK, p38, ERK 1/2) pathways. This compound inhibits the production of pro-inflammatory cytokines and the activity of COX-2 and iNOS and reduces the generation of reactive oxygen species [71,72]. Similarly, *B. microphylla* contains phenolic compounds such as Kaempferol and Quercetin, which modulate the inflammatory response through various pathways, including the inhibition of pro-inflammatory cytokine production, reduction in oxidative stress, and modulation of NF-κB, MAPK, and Nrf2/Keap1/ARE signaling pathways [73]. These findings suggest that lignans and phenolic compounds may be the main contributors to the anti-inflammatory effect observed.

When comparing the extract with the micro-aerogels loaded with extract (CsMBT-0.5 and CsMBT-1), an improvement in the anti-inflammatory activity is observed. This suggests that the extract combination with the CS matrix has a synergistic effect, where CS acts not only as a support but also as an active agent. The anti-inflammatory properties of CS have been previously reported and are linked to its ability to interact with immune cells and modulate cytokine release [74]. Therefore, the incorporation of the extract into the CS matrix may enhance the anti-inflammatory response. *B. microphylla* may influence the MAPK signaling pathway, possibly altering the phosphorylation of ERK and p38, which play key roles in regulating inflammatory responses [75]. Thus, the anti-inflammatory effect of the *B. microphylla* stem extract may be associated with its ability to inhibit the MAPK pathway.

CD1 mouse model was used to analyze the healing activity because they do not exhibit delayed wound healing, which allows for a more accurate assessment of the efficacy of experimental treatments [76]. This model is useful for observing wound healing, as their skin anatomy and wound contraction ability are more representative of the physiological response expected in rapid healing situations [77].

The assessment of healing activity highlighted the effectiveness of micro-aerogels and *B. microphylla* extract in reducing wound size, which is crucial for accelerating the healing process (see Figures 9 and 10). It is noteworthy that the early reduction in wound area observed with CsMBT-0.5 from the first day of treatment is particularly significant, as rapid wound closure not only minimizes the risk of pathogen invasion but also facilitates fibroblast migration and granulation tissue formation [78]. This underscores the importance of using formulations that promote a rapid response in the healing process [79]. Micro-aerogel-based formulations, particularly in the later stages (days 6, 9, and 12), show an improved performance compared to the commercial healing agent KitosCell-Q, emphasizing the significance of the physicochemical properties of these materials in their therapeutic efficacy. This advantage is mainly due to the ability of micro-aerogels to provide a sustained release profile of the active compounds, thereby enhancing their interaction with the wound site over time. The porous structure of the micro-aerogels also supports wound healing by creating a favorable environment for cell adhesion and migration, enabling efficient nutrient exchange and waste removal, which are essential for tissue regeneration [80].

When analyzing the healing activity of the micro-aerogels and their components, both chitosan and *B. microphylla* extract offer complementary effects. Chitosan, recognized for its healing properties, promotes tissue regeneration by interacting with growth factors and providing a support matrix that facilitates cell adhesion and migration [81]. Furthermore, its ability to reduce inflammation by modulating cytokine release reinforces its value in wound care, as confirmed by the significant reduction in wound area observed with CsM [82].

The wound-healing effect of the *B. microphylla* extract could be attributed to its bioactive compounds, including lignans such as Hinokinin and Burseran and phenolics like Kaempferol and Quercetin. These compounds have been shown to help modulate inflammation and reduce oxidative stress, which could facilitate tissue regeneration. While the extract alone promotes wound closure by day 12, the micro-aerogel formulation, with its controlled release mechanism, may further enhance these effects. This suggests that the combination of these bioactive compounds, along with the sustained release system, could significantly contribute to the observed healing activity. Together, this approach could accelerate wound closure and promote tissue regeneration, particularly in environments affected by chronic inflammation and oxidative stress [83].

In CD1 mice, wound healing could be primarily associated with wound contraction [84]. This is due to differences in their skin anatomy compared to humans, particularly the presence of a panniculus carnosus, a layer of striated muscle located between the subcutaneous adipose tissue and the interstitial connective tissue. This layer allows the rodent's skin to be looser relative to the underlying muscle, facilitating wound contraction during healing [85]. Therefore, the treatments evaluated, such as CsM with *B. microphylla* extract, could modulate this contraction ability, contributing to the reduction in the observed wound size.

Previous research has analyzed the wound-healing activities of various formulations and natural compounds. *Aloe vera*-based hydrogels have shown positive effects on inflammation, angiogenesis, and wound contraction, reducing the total healing time by 29% and achieving complete wound closure within 15 days. These results were obtained using a female Wistar rat model [86]. On the other hand, chitosan hydrogels combined with Aloe vera and *Calendula officinalis* extracts demonstrated 40% wound closure on the first day in a Wistar rat model, highlighting their anti-inflammatory and antioxidant effects alongside the regenerative capacity of chitosan [87]. These studies provide a solid context to compare the effect of *Bursera microphylla* extracts and their micro-aerogels, emphasizing their competitive potential as an innovative therapeutic alternative.

However, it is essential to consider that the variability in the chemical composition of *B. microphylla*, influenced by environmental factors or harvesting methods, could lead to inconsistencies in therapeutic effects, which would affect the reproducibility of the results. The concentration of bioactive compounds, such as lignans and phenolics, might vary between extract batches, further complicating the interpretation of therapeutic outcomes.

4. Materials and Methods

4.1. Plant Material

B. microphylla specimens were collected in Caborca, Sonora, in the 'La Proveedora' area along the Mexico 2 international highway, section Caborca-La Y Griega, during the spring of 2023 (30.683562, −112.273147). The collection was carried out randomly, obtaining a weight of 640 g for the stems. The plant *B. microphylla* was identified at the Herbarium of the University of Sonora by Dr. Manuel Higinio Sandoval Ortega, with a voucher specimen number 30333 [37].

4.2. Generation of Ethanolic Extracts

The stems were ground into a fine powder. The plant material was then extracted with ethanol (1:10 *w*/*v*) at room temperature for 10 days with brief manual agitation. The extracts were filtered and dried at 45 °C under reduced pressure. The resulting ethanolic extracts were stored at 4 °C until use [37].

4.3. Chitosan Preparation

Medium molecular weight chitosan (190,000 Da) (Sigma-Aldrich, 448,877, Toluca, México), 0.3 M acetic acid, glacial acetic acid (≥99.5% purity), and acetone (≥99.5% purity) were used. A 2% (*w*/*w*) chitosan solution was prepared by dissolving chitosan in an aqueous solution of 0.3 M acetic acid at room temperature and stirring for 24 h. Ammonium hydroxide at 28% was used to cross-link the chitosan structures. All reagents were purchased from Sigma-Aldrich [29].

4.4. Physical Cross-Linking of Chitosan Aerogels and Micro-Aerogels

After homogenizing, the chitosan solution was placed into 10 mL beakers with 1.5 g of the chitosan solution, and 0.18 g (1.0%) and 0.09 g (0.5%) of the ethanolic extract of *B. microphylla* stems were added. The beakers were then placed in a sealed chamber with ammonium hydroxide for 24 h. Physical cross-linking (gelation) was induced by the diffusion of ammonia [88]. The resulting hydrogels were washed with distilled water (500 mL × 3) to remove ammonium acetate and excess ammonium hydroxide until a pH of 7 was reached. To create three-dimensional structures, the hydrogels were frozen at −20 °C and then lyophilized using a LABCONCO 4.5 FreeZone freeze dryer at −53 °C and 0.016 mBar pressure for 24 h. This process formed pores in the chitosan, transforming it into a physically stable material known as an aerogel [65].

Three types of aerogels were obtained: CsA (made only with chitosan); CsABT-0.5 (loaded with 0.5% ethanolic extract of *B. microphylla* stems); and CsABT-1 (loaded with 1% extract of *B. microphylla* stems). These materials were mechanically ground to produce particulate materials known as micro-aerogels: CsM (made only with chitosan); CsMBT-0.5 (loaded with 0.5% *B. microphylla* stem extract); and CsMBT-1 (loaded with 1% *B. microphylla* stem extract). The materials were stored in a desiccator at room temperature until use.

4.5. Physicochemical Characterization of Chitosan Materials

4.5.1. Optical Microscopy and Scanning Electron Microscopy

The size and morphology of the micro-aerogels (CsM, CsMBT-0.5, CsMBT-1) were analyzed using optical microscopy (OM) and scanning electron microscopy (SEM). The apparent length of the microparticles was measured using a LABOMED CX microscope with a 12 V 20 W lamp (Labo America, Inc., Fremont, CA, USA) and an OEM object micrometer. For OM analysis, the scale on the ruler was 10 µm. SEM analysis was performed with a Hitachi SU8230 at 10 kV, where the microparticles were placed on aluminum tape and coated with a gold layer using a high-vacuum system Desk II (Denton Vacuum, Moorestown, NJ 08057, USA). SEM micrographs were taken at 200× with a scale of 200 µm [65].

4.5.2. Fourier-Transform Infrared Spectroscopy (FTIR)

Fourier-transform infrared spectroscopy (FTIR) was used to analyze the functional groups and bonds within the material's structure. It also provides information on the composition, crystallinity, orientation, and interaction of biomaterials [89,90]. The micro-aerogels were analyzed using a Perkin Elmer Spectrum Two FTIR spectrometer. The spectra were examined in the wavenumber range of 4000–650 cm^{-1} with a resolution of 4 cm^{-1} and a ratio of 100. To run this analysis, 6 mg of sample was used, and the spectra were

analyzed in the OriginPro 7 program without normalizing the data to see the appearance of new interactions [65].

4.5.3. Relative Humidity Absorption Analysis

To assess the moisture absorption capacity of the micro-aerogels, the specimens (15 mg sample per sample) were dried under reduced pressure for 2 days at 30 °C. Subsequently, the micro-aerogels were stored at two relative humidity (RH) levels: 40 ± 1% and 80 ± 1%, using 60 g of magnesium nitrate hexahydrate ($Mg(NO_3)_2 \cdot 6H_2O$) and 60 g of sodium sulfate decahydrate ($Na_2SO_4 \cdot 10H_2O$), respectively. The mass of each sample was measured at the beginning of this study and monitored over time until equilibrium was reached [29].

4.5.4. Thermogravimetric Analysis (TGA)

Thermogravimetric analysis (TGA) helps to understand the thermal decomposition mechanism and the stability of formulations at high temperatures. The thermogravimetric study was carried out using a Mettler Toledo TGA/DSC 2+ thermal analyzer under a nitrogen atmosphere. Micro-aerogels (6 mg per sample) were analyzed at temperatures ranging from 25 to 600 °C with a heating rate of 10 °C/min. The graphs were analyzed using OriginPro 7, and the derivative of the mass loss was added to the same graph for better interpretation [65].

4.6. Cell Culture

Macrophages transformed by Abelson leukemia virus (RAW264.7) were provided by Dr. Emil A. Unanue from the Department of Pathology and Immunology, Washington University, St. Louis, MO, USA. The RAW 264.7 cell line (A belson leukemia virus-induced murine macrophages) was cultured in DMEM (Dulbecco's modified Eagle's medium) supplemented with 5% heat-inactivated fetal bovine serum and penicillin (100 U/mL) in 25 cm^2 culture plates. Incubation was performed in an Isotherm incubator under the following conditions: 5% CO_2; 37 °C; and 95% relative humidity (Thermo Fisher Scientific, Waltham, MA, USA), with incubation times ranging from 24 to 48 h.

4.7. Cytotoxic Effect

The MTT assay (3-(4,5-dimethylthiazol-2-yl)-2,5-diphenyltetrazolium bromide) was used to evaluate the cytotoxic effects of the ethanolic extract from *B. microphylla* stems, as well as the micro-aerogels. RAW 264.7 cells were cultured until they reached 80% confluence, then detached through enzymatic digestion using 3 mL of trypsin and collected in DMEM. Subsequently, the cells were centrifuged (Beckman Coulter R Allegra X-15R with SX4750 rotor, Brea, CA, USA) for 7 min at 1700 rpm and 4 °C. The supernatant was discarded, and the cell pellet was resuspended with DMEM. A RAW 264.7 cells suspension was prepared (500,000 cells/mL), and 100 µL of this suspension (50,000 cells in each well) were plated in a 96-well plate (Costar, Corning, NY, USA) and incubated for 24 h. The cells were then treated with the extract (0.78–6.25 µg/mL) with or without LPS (lipopolysaccharide) for 24 h or micro-aerogels (12.5–100 µg/mL) with or without LPS (1 µg/mL) (0111, Sigma Aldrich) for 24 h by the indirect method (the microparticles were placed in a pH 5 buffer for 4 h, and then, 100 µL of the supernatant was taken to treat the cells). After washing with PBS 1X, the cells were incubated with an MTT solution (5 mg/mL) for 4 h. The formazan crystals were resuspended with acidic isopropanol, and absorbance readings were recorded at 570 and 630 nm using a BIO-RAD iMARK microplate reader. Cytotoxicity was expressed as a percentage, with untreated cells considered 100% viable, and treatments were deemed cytotoxic when viability was <90%. The experiments were performed in triplicate [91,92].

4.8. Effect on NO Production

The effect on NO production was evaluated in the supernatant of LPS-activated RAW 264.7 cells using the Griess reaction. A cell culture with a confluence of ≥90% was prepared into a suspension at a density of 500,000 cells/mL. Subsequently, 100 µL of the cell suspension (50,000 cells in each well) was added to a 96-well plate (Costar, Corning, NY, USA) and incubated for 24 h. The cells were then stimulated with LPS (1 µg/mL) in the presence or absence of *B. microphylla* extract (0.78–6.25 µg/mL) or micro-aerogels (12.5–100 µg/mL) for 24 h. Afterward, 100 µL of the supernatant was mixed with an equal volume of Griess reagent and incubated at room temperature for 10 min. Finally, absorbance was read at 540 nm using a microplate reader (iMARK microplate reader, BIO-RAD, Laboratories, México, D.F.). A standard nitrite curve was used to determine NO levels. The experiments were performed in triplicate [37].

4.9. Experimental Animals

The anti-inflammatory and wound-healing effects were analyzed in the skin wound model in CD1 female mice. CD1 mice were selected due to their outbred nature, which provides genetic diversity and a robust immune response, making them suitable for studying inflammation and wound-healing processes. Additionally, this strain is commonly used in dermatological and wound-healing studies [93]. The CD1 mice used in this study were provided by the Faculty of Medicine at the Autonomous University of the State of Morelos (UAEM). The CD1 mice were 13 to 15 weeks old, with a body weight of approximately 22–28 g. They were maintained on a 12/12-h light/dark cycle at a temperature of 24 °C. Food and water were provided ad libitum. All experimental procedures were conducted in compliance with the Mexican Official Standard NOM-062-ZOO-1999 and the protocol approved by the Research Ethics Committee of the University of Sonora (CEI-UNISON/1A-3-02/2024) [94].

4.10. Drugs and Reagents

For the anti-inflammatory model, a 0.9% physiological saline solution (SSF) was used as a vehicle for the micro-aerogels and *B. microphylla* extract. Indomethacin served as a positive control at a concentration of 0.30 mg/ear, known for its anti-inflammatory properties. Ear edema was induced by administering TPA (12-tetradecanoylphorbol-13-acetate) at 10 µg/ear, a standard technique for inducing inflammation in animal models. All treatments, including indomethacin, micro-aerogels, and the extract, were prepared on the experimental day to ensure proper administration and comparability of results [95].

4.11. TPA-Induced Ear Edema Model

The anti-inflammatory activity was assessed using the TPA-induced ear edema model. Mice were anesthetized with pentobarbital (63 mg/kg, intraperitoneally), and edema was induced by applying TPA (10 µg/ear). Indomethacin was dissolved in acetone prior to application. The positive control group received indomethacin at concentrations of 5 and 30 mg/mL immediately after TPA application. Micro-aerogels (30 mg/mL) and the *B. microphylla* extract were also dissolved in 0.9% SSF and applied topically to the right ear, along with the various treatments. A sample size of $n = 5$ was used for each treatment group [96].

4.12. Wound Healing Model

To evaluate the potential wound-healing effect of the *B. microphylla* extract and micro-aerogels, mice were anesthetized with pentobarbital (63 mg/kg, intraperitoneally). The fur on the back of the mouse was shaved, and a wound was created using a punch (6 mm). Once the wound was made, 10 µL of the treatments was applied to the wound using a

micropipette: 0.9% SSF (vehicle); CsMBT-0.5 (30 mg/mL); CsMBT-1.0 (30 mg/mL); ethanolic extract of *B. microphylla* stems (30 mg/mL); and KitosCell-Q (30 mg/mL) as a positive control for healing. The dose of 30 mg/mL for the ethanolic extract of *B. microphylla* and the micro-aerogels was selected based on preliminary studies and the previous literature on the effective concentrations for other plant extracts in wound healing models. This dose was chosen to provide a robust therapeutic effect while minimizing potential toxicity. Additionally, the selected dose corresponds to a safe and effective concentration when considering potential human applications [97]. After treatment, the mice were observed for 4 h to prevent any self-inflicted damage to the affected area. Healing kinetics were recorded with photographs taken every 3 days until day 18 post-injury. The wound area was measured using image analysis software (Image J® software v.1.5), and healing kinetics for each treatment were calculated. A sample size of $n = 5$ was used for each treatment group [98].

4.13. Statistical Analysis

The results from the in vitro studies were presented as mean ± standard deviation (SD) from three independent experiments. A one-way ANOVA was conducted to assess significant differences between experimental groups, followed by the Tukey multiple comparison test to pinpoint specific differences. In vivo data were also expressed as mean ± SD, with one-way ANOVA used to analyze ear weight and thickness differences. The Bonferroni test was applied post hoc for accuracy in multiple comparisons. For wound healing analysis, a two-way ANOVA was followed by Dunnett's post hoc test to compare the control and treatment groups at various time points [98].

5. Conclusions

In this study, it has been demonstrated that chitosan-based micro-aerogels loaded with *B. microphylla* extract represent a promising alternative to address these challenges. The research revealed that these micro-aerogels not only exhibit optimal physicochemical characteristics, such as a highly porous structure and thermal stability, but also facilitate the controlled release of bioactive compounds. This contributes to reducing inflammation and fostering a favorable environment for tissue regeneration. The results indicate that the formulation of the micro-aerogels significantly improves cell viability and enhances anti-inflammatory activity, suggesting a synergistic effect between chitosan and *B. microphylla* extract. However, it is important to highlight that the extract itself also shows promising results, particularly in modulating inflammation and promoting wound closure. The ability of both the extract and the micro-aerogels to accelerate wound closure underscores their therapeutic potential in treating complicated injuries, particularly those associated with chronic inflammation and oxidative stress. Chitosan micro-aerogels, combined with *B. microphylla* extract, represent an innovative and effective approach to modulating inflammation and improving wound healing, opening new perspectives for their application in regenerative therapies and the development of more effective treatments for wound management.

Future Prospects

Future studies should focus on preclinical trials to confirm the effectiveness and safety of the micro-aerogels and *B. microphylla extract*. Additionally, exploring the antimicrobial properties of *B. microphylla* could open new possibilities for its therapeutic application in treating infections, which could further enhance wound healing treatments. It would also be valuable to know in more detail the phytochemical profile of *B. microphylla* to isolate and characterize the bioactive compounds present, which could help optimize formulations and provide a better understanding of the mechanisms of action involved in its therapeutic activity.

Author Contributions: Investigation, methodology, and validation, J.R.C.-O., J.J.A.-F., J.C.L.-R., R.E.R.-Z., V.A.R.-U. and H.T.-M.; writing—review and editing, J.J.A.-F., J.C.L.-R., V.A.R.-U. and H.T.-M.; data curation and validation, J.R.C.-O., J.C.L.-R., V.A.R.-U. and H.T.-M.; writing—original draft preparation, conceptualization, investigation, resources, and supervision, J.J.A.-F., J.C.L.-R., R.E.R.-Z. and H.T.-M. All authors have read and agreed to the published version of the manuscript.

Funding: This research is funded by the Consejo Nacional de Humanidades Ciencias y Tecnologías (CONAHCYT) with the project CBF-2023-2024-3824, Ciencia Básica y de Frontera 2023–2024, Mexico.

Data Availability Statement: Data are contained within the article.

Acknowledgments: Juan R. Cañez-Orozco thanks CONAHCYT for the support provided. He also expresses his gratitude to the University of Sonora, Hermosillo, and Caborca campuses for providing the necessary facilities to conduct this research. We additionally thank Juan J. Acevedo-Fernández for his valuable assistance with the animal model analyses.

Conflicts of Interest: The authors declare no conflicts of interest.

References

1. Han, G.; Ceilley, R. Chronic Wound Healing: A Review of Current Management and Treatments. *Adv. Ther.* **2017**, *34*, 599–610. [CrossRef] [PubMed]
2. Takeo, M.; Lee, W.; Ito, M. Wound Healing and Skin Regeneration. *Cold Spring Harb. Perspect. Med.* **2015**, *5*, a023267. [CrossRef] [PubMed]
3. Rodrigues, M.; Kosaric, N.; Bonham, C.A.; Gurtner, G.C. Wound Healing: A Cellular Perspective. *Physiol. Rev.* **2019**, *99*, 665–706. [CrossRef]
4. Wang, P.-H.; Huang, B.-S.; Horng, H.-C.; Yeh, C.-C.; Chen, Y.-J. Wound Healing. *J. Chin. Med. Assoc.* **2018**, *81*, 94–101. [CrossRef] [PubMed]
5. Guimarães, M.E.A.; Derhon, V.; Signori, L.U.; Seiffer, B.A.; Wolf, S.; Schuch, F.B. Acute and Chronic Effects of Physical Exercise in Inflammatory Biomarkers in People with Depression: A Systematic Review with Meta-Analysis. *J. Psychiatr. Res.* **2024**, *179*, 26–32. [CrossRef]
6. Gonçalves, R.V.; Freitas, M.B.; Esposito, D. Cellular and Molecular Mechanisms of Oxidative Stress in Wound Healing. *Oxidative Med. Cell. Longev.* **2022**, *2022*, 9785094. [CrossRef]
7. Joffre, J.; Hellman, J. Oxidative Stress and Endothelial Dysfunction in Sepsis and Acute Inflammation. *Antioxid. Redox Signal.* **2021**, *35*, 1291–1307. [CrossRef] [PubMed]
8. Huang, J.; Heng, S.; Zhang, W.; Liu, Y.; Xia, T.; Ji, C.; Zhang, L. Dermal Extracellular Matrix Molecules in Skin Development, Homeostasis, Wound Regeneration and Diseases. *Semin. Cell Dev. Biol.* **2022**, *128*, 137–144. [CrossRef]
9. Wilkinson, H.N.; Hardman, M.J. Wound Healing: Cellular Mechanisms and Pathological Outcomes. *Open Biol.* **2020**, *10*, 200223. [CrossRef]
10. Martin, P.; Nunan, R. Cellular and Molecular Mechanisms of Repair in Acute and Chronic Wound Healing. *Br. J. Dermatol.* **2015**, *173*, 370–378. [CrossRef] [PubMed]
11. Raziyeva, K.; Kim, Y.; Zharkinbekov, Z.; Kassymbek, K.; Jimi, S.; Saparov, A. Immunology of Acute and Chronic Wound Healing. *Biomolecules* **2021**, *11*, 700. [CrossRef]
12. Ko, K.I.; Sculean, A.; Graves, D.T. Diabetic Wound Healing in Soft and Hard Oral Tissues. *Transl. Res.* **2021**, *236*, 72–86. [CrossRef]
13. Alma, A.; Marconi, G.D.; Rossi, E.; Magnoni, C.; Paganelli, A. Obesity and Wound Healing: Focus on Mesenchymal Stem Cells. *Life* **2023**, *13*, 717. [CrossRef] [PubMed]
14. Mosser, D.M.; Hamidzadeh, K.; Goncalves, R. Macrophages and the Maintenance of Homeostasis. *Cell. Mol. Immunol.* **2021**, *18*, 579–587. [CrossRef] [PubMed]
15. Deng, L.; Du, C.; Song, P.; Chen, T.; Rui, S.; Armstrong, D.G.; Deng, W. The Role of Oxidative Stress and Antioxidants in Diabetic Wound Healing. *Oxidative Med. Cell. Longev.* **2021**, *2021*, 8852759. [CrossRef] [PubMed]
16. Wang, G.; Yang, F.; Zhou, W.; Xiao, N.; Luo, M.; Tang, Z. The Initiation of Oxidative Stress and Therapeutic Strategies in Wound Healing. *Biomed. Pharmacother.* **2023**, *157*, 114004. [CrossRef]
17. Chang, R.W.; Tompkins, D.M.; Cohn, S.M. Are NSAIDs Safe? Assessing the Risk-Benefit Profile of Nonsteroidal Anti-Inflammatory Drug Use in Postoperative Pain Management. *Am. Surg.* **2021**, *87*, 872–879. [CrossRef]
18. Ribeiro, H.; Rodrigues, I.; Napoleão, L.; Lira, L.; Marques, D.; Veríssimo, M.; Andrade, J.P.; Dourado, M. Non-Steroidal Anti-Inflammatory Drugs (NSAIDs), Pain and Aging: Adjusting Prescription to Patient Features. *Biomed. Pharmacother.* **2022**, *150*, 112958. [CrossRef] [PubMed]

19. Namjoshi, S.; Dabbaghi, M.; Roberts, M.S.; Grice, J.E.; Mohammed, Y. Quality by Design: Development of the Quality Target Product Profile (QTPP) for Semisolid Topical Products. *Pharmaceutics* **2020**, *12*, 287. [CrossRef]
20. Parolini, M. Toxicity of the Non-Steroidal Anti-Inflammatory Drugs (NSAIDs) Acetylsalicylic Acid, Paracetamol, Diclofenac, Ibuprofen and Naproxen towards Freshwater Invertebrates: A Review. *Sci. Total Environ.* **2020**, *740*, 140043. [CrossRef] [PubMed]
21. Bindu, S.; Mazumder, S.; Bandyopadhyay, U. Non-Steroidal Anti-Inflammatory Drugs (NSAIDs) and Organ Damage: A Current Perspective. *Biochem. Pharmacol.* **2020**, *180*, 114147. [CrossRef] [PubMed]
22. Jin, X.; Imran, M.; Mohammed, Y. Topical Semisolid Products—Understanding the Impact of Metamorphosis on Skin Penetration and Physicochemical Properties. *Pharmaceutics* **2022**, *14*, 2487. [CrossRef] [PubMed]
23. Zielińska, A.; Eder, P.; Rannier, L.; Cardoso, J.C.; Severino, P.; Silva, A.M.; Souto, E.B. Hydrogels for Modified-Release Drug Delivery Systems. *Curr. Pharm. Des.* **2022**, *28*, 609–618. [CrossRef] [PubMed]
24. Wang, X.; Song, R.; Johnson, M.; Sigen, A.; Shen, P.; Zhang, N.; Lara-Sáez, I.; Xu, Q.; Wang, W. Chitosan-Based Hydrogels for Infected Wound Treatment. *Macromol. Biosci.* **2023**, *23*, e2300094. [CrossRef] [PubMed]
25. Abd El-Hack, M.E.; El-Saadony, M.T.; Shafi, M.E.; Zabermawi, N.M.; Arif, M.; Batiha, G.E.; Khafaga, A.F.; Abd El-Hakim, Y.M.; Al-Sagheer, A.A. Antimicrobial and Antioxidant Properties of Chitosan and Its Derivatives and Their Applications: A Review. *Int. J. Biol. Macromol.* **2020**, *164*, 2726–2744. [CrossRef]
26. Jyoti, K.; Malik, G.; Chaudhary, M.; Sharma, M.; Goswami, M.; Katare, O.P.; Singh, S.B.; Madan, J. Chitosan and Phospholipid Assisted Topical Fusidic Acid Drug Delivery in Burn Wound: Strategies to Conquer Pharmaceutical and Clinical Challenges, Opportunities and Future Panorama. *Int. J. Biol. Macromol.* **2020**, *161*, 325–335. [CrossRef]
27. Alven, S.; Aderibigbe, B.A. Chitosan and Cellulose-Based Hydrogels for Wound Management. *Int. J. Mol. Sci.* **2020**, *21*, 9656. [CrossRef]
28. Behr, M.; Ganesan, K. Improving Polysaccharide-Based Chitin/Chitosan-Aerogel Materials by Learning from Genetics and Molecular Biology. *Materials* **2022**, *15*, 1041. [CrossRef] [PubMed]
29. Reyna-Urrutia, V.A.; Mata-Haro, V.; Cauich-Rodriguez, J.V.; Herrera-Kao, W.A.; Cervantes-Uc, J.M. Effect of Two Crosslinking Methods on the Physicochemical and Biological Properties of the Collagen-Chitosan Scaffolds. *Eur. Polym. J.* **2019**, *117*, 424–433. [CrossRef]
30. Shi, W.; Ching, Y.C.; Chuah, C.H. Preparation of Aerogel Beads and Microspheres Based on Chitosan and Cellulose for Drug Delivery: A Review. *Int. J. Biol. Macromol.* **2021**, *170*, 751–767. [CrossRef] [PubMed]
31. Kulkarni, P.G.; Paudel, N.; Magar, S.; Santilli, M.F.; Kashyap, S.; Baranwal, A.K.; Zamboni, P.; Vasavada, P.; Katiyar, A.; Singh, A.V. Overcoming Challenges and Innovations in Orthopedic Prosthesis Design: An Interdisciplinary Perspective. *Biomed. Mater. Devices* **2023**, *2*, 58–69. [CrossRef] [PubMed]
32. Pacyga, K.; Pacyga, P.; Topola, E.; Viscardi, S.; Duda-Madej, A. Bioactive Compounds from Plant Origin as Natural Antimicrobial Agents for the Treatment of Wound Infections. *Int. J. Mol. Sci.* **2024**, *25*, 2100. [CrossRef] [PubMed]
33. Yazarlu, O.; Iranshahi, M.; Kashani, H.R.K.; Reshadat, S.; Habtemariam, S.; Iranshahy, M.; Hasanpour, M. Perspective on the Application of Medicinal Plants and Natural Products in Wound Healing: A Mechanistic Review. *Pharmacol. Res.* **2021**, *174*, 105841. [CrossRef]
34. Salazar-Gómez, A.; Alonso-Castro, A.J. Medicinal Plants from Latin America with Wound Healing Activity: Ethnomedicine, Phytochemistry, Preclinical and Clinical Studies—A Review. *Pharmaceuticals* **2022**, *15*, 1095. [CrossRef] [PubMed]
35. Felger, R.S.; Moser, M.B. Seri Indian Pharmacopoeia. *Econ. Bot.* **1973**, *28*, 415–436. [CrossRef]
36. Gigliarelli, G.; Zadra, C.; Cossignani, L.; Robles Zepeda, R.E.; Rascón-Valenzuela, L.A.; Velázquez-Contreras, C.A.; Marcotullio, M.C. Two New Lignans from the Resin of Bursera Microphylla A. Gray and Their Cytotoxic Activity. *Nat. Prod. Res.* **2018**, *32*, 2646–2651. [CrossRef] [PubMed]
37. Torres-Moreno, H.; López-Romero, J.C.; Vidal-Gutiérrez, M.; Rodríguez-Martínez, K.L.; Robles-Zepeda, R.E.; Vilegas, W.; Velarde-Rodríguez, G.M. Seasonality Impact on the Anti-Inflammatory, Antiproliferative Potential and the Lignan Composition of Bursera Microphylla. *Ind. Crops Prod.* **2022**, *184*, 115095. [CrossRef]
38. Messina, F.; Curini, M.; Di Sano, C.; Zadra, C.; Gigliarelli, G.; Rascón-Valenzuela, L.A.; Robles Zepeda, R.E.; Marcotullio, M.C. Diterpenoids and Triterpenoids from the Resin of Bursera Microphylla and Their Cytotoxic Activity. *J. Nat. Prod.* **2015**, *78*, 1184–1188. [CrossRef]
39. Xu, J.; Song, W.; Wu, N.; Tong, J.; Ren, L. Preparation and Characterization of Chitosan/Polyvinyl Porous Alcohol Aerogel Microspheres with Stable Physicochemical Properties. *Int. J. Biol. Macromol.* **2021**, *187*, 614–623. [CrossRef]
40. Savic, I.M.; Savic Gajic, I.M.; Milovanovic, M.G.; Zerajic, S.; Gajic, D.G. Optimization of Ultrasound-Assisted Extraction and Encapsulation of Antioxidants from Orange Peels in Alginate-Chitosan Microparticles. *Antioxidants* **2022**, *11*, 297. [CrossRef]
41. Do, N.H.N.; Huynh, T.N.A.; Le, T.X.; Ha, A.C.; Le, P.K. Encapsulation of Triphasia Trifolia Extracts by pH and Thermal Dual-Sensitive Chitosan Hydrogels for Controlled Release. *Carbohydr. Polym.* **2023**, *320*, 121264. [CrossRef] [PubMed]

42. Detsi, A.; Kavetsou, E.; Kostopoulou, I.; Pitterou, I.; Pontillo, A.R.N.; Tzani, A.; Christodoulou, P.; Siliachli, A.; Zoumpoulakis, P. Nanosystems for the Encapsulation of Natural Products: The Case of Chitosan Biopolymer as a Matrix. *Pharmaceutics* **2020**, *12*, 669. [CrossRef]
43. Hameed, H.; Faheem, S.; Paiva-Santos, A.C.; Sarwar, H.S.; Jamshaid, M. A Comprehensive Review of Hydrogel-Based Drug Delivery Systems: Classification, Properties, Recent Trends, and Applications. *AAPS PharmSciTech* **2024**, *25*, 64. [CrossRef]
44. Kamal Mohamed, S.M.; Heinrich, C.; Milow, B. Effect of Process Conditions on the Properties of Resorcinol-Formaldehyde Aerogel Microparticles Produced via Emulsion-Gelation Method. *Polymers* **2021**, *13*, 2409. [CrossRef]
45. Nikulenkova, O.V.; Krupnin, A.E.; Dmitryakov, P.V.; Zagoskin, Y.D.; Malakhov, S.N.; Grigoriev, T.E.; Kuznetsov, N.M.; Chvalun, S.N. Mechanical Properties of Individual Porous Chitosan Particles: Full Scale and Numerical Experiments. *Nanotechnol Russ.* **2024**, *19*, 258–265. [CrossRef]
46. Lekhavadhani, S.; Shanmugavadivu, A.; Selvamurugan, N. Role and Architectural Significance of Porous Chitosan-Based Scaffolds in Bone Tissue Engineering. *Int. J. Biol. Macromol.* **2023**, *251*, 126238. [CrossRef]
47. Hoffmann, B.; Seitz, D.; Mencke, A.; Kokott, A.; Ziegler, G. Glutaraldehyde and Oxidised Dextran as Crosslinker Reagents for Chitosan-Based Scaffolds for Cartilage Tissue Engineering. *J. Mater. Sci. Mater. Med.* **2009**, *20*, 1495–1503. [CrossRef] [PubMed]
48. Malheiro, V.N.; Caridade, S.G.; Alves, N.M.; Mano, J.F. New Poly(ε-Caprolactone)/Chitosan Blend Fibers for Tissue Engineering Applications. *Acta Biomater.* **2010**, *6*, 418–428. [CrossRef] [PubMed]
49. Santos-López, G.; Argüelles-Monal, W.; Carvajal-Millan, E.; López-Franco, Y.; Recillas-Mota, M.; Lizardi-Mendoza, J. Aerogels from Chitosan Solutions in Ionic Liquids. *Polymers* **2017**, *9*, 722. [CrossRef]
50. Thein-Han, W.W.; Misra, R.D.K. Biomimetic Chitosan–Nanohydroxyapatite Composite Scaffolds for Bone Tissue Engineering. *Acta Biomater.* **2009**, *5*, 1182–1197. [CrossRef] [PubMed]
51. Szymańska, E.; Winnicka, K. Stability of Chitosan—A Challenge for Pharmaceutical and Biomedical Applications. *Mar. Drugs* **2015**, *13*, 1819–1846. [CrossRef]
52. Gao, Y.; Xie, Y.; Sun, H.; Zhao, Q.; Zheng, X.; Wang, S.; Jiang, T. Effect of Pore Size of Three-Dimensionally Ordered Macroporous Chitosan–Silica Matrix on Solubility, Drug Release, and Oral Bioavailability of Loaded-Nimodipine. *Drug Dev. Ind. Pharm.* **2016**, *42*, 464–472. [CrossRef] [PubMed]
53. Xu, B.; Zhang, Z.; Liang, H.; Hu, J.; Chen, L.; Wang, Z.; Chai, B.; Fan, G. Polyimide Aerogels with Low Thermal Conductivity and High-Temperature Stable Properties Prepared by Lyophilization for Flexible Thermal Protection. *High Perform. Polym.* **2024**, *36*, 42–51. [CrossRef]
54. Suenaga, S.; Osada, M. Preparation of β-Chitin Nanofiber Aerogels by Lyophilization. *Int. J. Biol. Macromol.* **2019**, *126*, 1145–1149. [CrossRef] [PubMed]
55. Li, L.; Li, Y.; Li, M.; Sun, Y.; Wang, H.; Cui, M.; Xu, W. Adsorption of Tetracycline by *Nicandra physaloides* (L.) *Gaertn* Seed Gum and *Nicandra physaloides(L.) Gaertn* Seed Gum/Carboxymethyl Chitosan Aerogel. *Environ. Technol.* **2022**, *43*, 4237–4248. [CrossRef] [PubMed]
56. Denizot, F.; Lang, R. Rapid Colorimetric Assay for Cell Growth and Survival. *J. Immunol. Methods* **1986**, *89*, 271–277. [CrossRef] [PubMed]
57. Sułkowska-Ziaja, K.; Robak, J.; Szczepkowski, A.; Gunia-Krzyżak, A.; Popiół, J.; Piotrowska, J.; Rospond, B.; Szewczyk, A.; Kała, K.; Muszyńska, B. Comparison of Bioactive Secondary Metabolites and Cytotoxicity of Extracts from Inonotus Obliquus Isolates from Different Host Species. *Molecules* **2023**, *28*, 4907. [CrossRef]
58. Sorg, H.; Tilkorn, D.J.; Hager, S.; Hauser, J.; Mirastschijski, U. Skin Wound Healing: An Update on the Current Knowledge and Concepts. *Eur. Surg. Res.* **2017**, *58*, 81–94. [CrossRef] [PubMed]
59. Peña, O.A.; Martin, P. Cellular and Molecular Mechanisms of Skin Wound Healing. *Nat. Rev. Mol. Cell Biol.* **2024**, *25*, 599–616. [CrossRef] [PubMed]
60. Hassanshahi, A.; Moradzad, M.; Ghalamkari, S.; Fadaei, M.; Cowin, A.J.; Hassanshahi, M. Macrophage-Mediated Inflammation in Skin Wound Healing. *Cells* **2022**, *11*, 2953. [CrossRef] [PubMed]
61. Antonangeli, F.; Grimsholm, O.; Rossi, M.N.; Velotti, F. Editorial: Cellular Stress and Inflammation: How the Immune System Drives Tissue Homeostasis. *Front. Immunol.* **2021**, *12*, 668876. [CrossRef] [PubMed]
62. Johnson, J.B.; Broszczak, D.A.; Mani, J.S.; Anesi, J.; Naiker, M. A Cut above the Rest: Oxidative Stress in Chronic Wounds and the Potential Role of Polyphenols as Therapeutics. *J. Pharm. Pharmacol.* **2022**, *74*, 485–502. [CrossRef] [PubMed]
63. Ferreira-Gonçalves, T.; Constantin, C.; Neagu, M.; Reis, C.P.; Sabri, F.; Simón-Vázquez, R. Safety and Efficacy Assessment of Aerogels for Biomedical Applications. *Biomed. Pharmacother.* **2021**, *144*, 112356. [CrossRef] [PubMed]
64. Reyna-Urrutia, V.A.; Robles-Zepeda, R.E.; Estevez, M.; Gonzalez-Reyna, M.A.; Alonso-Martínez, G.V.; Cáñez-Orozco, J.R.; López-Romero, J.C.; Torres-Moreno, H. Microparticles Loaded with Bursera Microphylla A. Gray Fruit Extract with Anti-Inflammatory and Antimicrobial Activity. *Pharmaceuticals* **2024**, *17*, 1565. [CrossRef]

65. Reyna-Urrutia, V.A.; Estevez, M.; González-González, A.M.; Rosales-Ibáñez, R. 3D Scaffolds of Caprolactone/Chitosan/Polyvinyl Alcohol/Hydroxyapatite Stabilized by Physical Bonds Seeded with Swine Dental Pulp Stem Cell for Bone Tissue Engineering. *J. Mater. Sci. Mater. Med.* **2022**, *33*, 81. [CrossRef] [PubMed]
66. Ulker, Z.; Erkey, C. An Emerging Platform for Drug Delivery: Aerogel Based Systems. *J. Control. Release* **2014**, *177*, 51–63. [CrossRef] [PubMed]
67. Man, M.-Q.; Wakefield, J.S.; Mauro, T.M.; Elias, P.M. Regulatory Role of Nitric Oxide in Cutaneous Inflammation. *Inflammation* **2022**, *45*, 949–964. [CrossRef] [PubMed]
68. Chotphruethipong, L.; Chanvorachote, P.; Reudhabibadh, R.; Singh, A.; Benjakul, S.; Roytrakul, S.; Hutamekalin, P. Chitooligosaccharide from Pacific White Shrimp Shell Chitosan Ameliorates Inflammation and Oxidative Stress via NF-κB, Erk1/2, Akt and Nrf2/HO-1 Pathways in LPS-Induced RAW264.7 Macrophage Cells. *Foods* **2023**, *12*, 2740. [CrossRef]
69. Jang, W.Y.; Kim, M.-Y.; Cho, J.Y. Antioxidant, Anti-Inflammatory, Anti-Menopausal, and Anti-Cancer Effects of Lignans and Their Metabolites. *Int. J. Mol. Sci.* **2022**, *23*, 15482. [CrossRef]
70. Ge, J.; Liu, Z.; Zhong, Z.; Wang, L.; Zhuo, X.; Li, J.; Jiang, X.; Ye, X.-Y.; Xie, T.; Bai, R. Natural Terpenoids with Anti-Inflammatory Activities: Potential Leads for Anti-Inflammatory Drug Discovery. *Bioorganic Chem.* **2022**, *124*, 105817. [CrossRef]
71. Lu, Q.; Zheng, R.; Zhu, P.; Bian, J.; Liu, Z.; Du, J. Hinokinin Alleviates High Fat Diet/Streptozotocin-Induced Cardiac Injury in Mice through Modulation in Oxidative Stress, Inflammation and Apoptosis. *Biomed. Pharmacother.* **2021**, *137*, 111361. [CrossRef]
72. Khazdair, M.R.; Anaeigoudari, A.; Agbor, G.A. Anti-Viral and Anti-Inflammatory Effects of Kaempferol and Quercetin and COVID-2019: A Scoping Review. *Asian Pac. J. Trop. Biomed.* **2021**, *11*, 327–334. [CrossRef]
73. Azeem, M.; Hanif, M.; Mahmood, K.; Ameer, N.; Chughtai, F.R.S.; Abid, U. An Insight into Anticancer, Antioxidant, Antimicrobial, Antidiabetic and Anti-Inflammatory Effects of Quercetin: A Review. *Polym. Bull.* **2023**, *80*, 241–262. [CrossRef] [PubMed]
74. Ayaz, F.; Demir, D.; Bölgen, N. Differential Anti-Inflammatory Properties of Chitosan-Based Cryogel Scaffolds Depending on Chitosan/Gelatin Ratio. *Artif. Cells Nanomed. Biotechnol.* **2021**, *49*, 682–690. [CrossRef]
75. Adorisio, S.; Fierabracci, A.; Gigliarelli, G.; Muscari, I.; Cannarile, L.; Liberati, A.M.; Marcotullio, M.C.; Riccardi, C.; Curini, M.; Robles Zepeda, R.E.; et al. The Hexane Fraction of *Bursera microphylla* A Gray Induces P21-Mediated Antiproliferative and Proapoptotic Effects in Human Cancer–Derived Cell Lines. *Integr. Cancer Ther.* **2017**, *16*, 426–435. [CrossRef] [PubMed]
76. Shagdarova, B.; Konovalova, M.; Zhuikova, Y.; Lunkov, A.; Zhuikov, V.; Khaydapova, D.; Il'ina, A.; Svirshchevskaya, E.; Varlamov, V. Collagen/Chitosan Gels Cross-Linked with Genipin for Wound Healing in Mice with Induced Diabetes. *Materials* **2022**, *15*, 15. [CrossRef] [PubMed]
77. Espinosa-Espinosa, L.; Garduño-Siciliano, L.; Rodriguez-Canales, M.; Hernandez-Portilla, L.B.; Canales-Martinez, M.M.; Rodriguez-Monroy, M.A. The Wound-Healing Effect of Mango Peel Extract on Incision Wounds in a Murine Model. *Molecules* **2022**, *27*, 259. [CrossRef]
78. Vivcharenko, V.; Trzaskowska, M.; Przekora, A. Wound Dressing Modifications for Accelerated Healing of Infected Wounds. *Int. J. Mol. Sci.* **2023**, *24*, 7193. [CrossRef] [PubMed]
79. Guo, B.; Dong, R.; Liang, Y.; Li, M. Haemostatic Materials for Wound Healing Applications. *Nat. Rev. Chem.* **2021**, *5*, 773–791. [CrossRef]
80. Grzybek, P.; Jakubski, Ł.; Dudek, G. Neat Chitosan Porous Materials: A Review of Preparation, Structure Characterization and Application. *Int. J. Mol. Sci.* **2022**, *23*, 9932. [CrossRef] [PubMed]
81. Guo, S.; Ren, Y.; Chang, R.; He, Y.; Zhang, D.; Guan, F.; Yao, M. Injectable Self-Healing Adhesive Chitosan Hydrogel with Antioxidative, Antibacterial, and Hemostatic Activities for Rapid Hemostasis and Skin Wound Healing. *ACS Appl. Mater. Interfaces* **2022**, *14*, 34455–34469. [CrossRef] [PubMed]
82. Narvaez-Flores, J.; Vilar-Pineda, G.; Acosta-Torres, L.; Garcia-Contreras, R. Cytotoxic and Anti-Inflammatory Effects of Chitosan and Hemostatic Gelatin in Oral Cell Culture. *Acta Odontol. Latinoam.* **2021**, *34*, 98–103. [CrossRef]
83. Yoshida, C.M.P.; Pacheco, M.S.; de Moraes, M.A.; Lopes, P.S.; Severino, P.; Souto, E.B.; da Silva, C.F. Effect of Chitosan and Aloe Vera Extract Concentrations on the Physicochemical Properties of Chitosan Biofilms. *Polymers* **2021**, *13*, 1187. [CrossRef] [PubMed]
84. Saeed, S.; Martins-Green, M. Animal Models for the Study of Acute Cutaneous Wound Healing. *Wound Repair Regen.* **2023**, *31*, 6–16. [CrossRef] [PubMed]
85. Chen, L.; Mirza, R.; Kwon, Y.; DiPietro, L.A.; Koh, T.J. The Murine Excisional Wound Model: Contraction Revisited. *Wound Repair Regen.* **2015**, *23*, 874–877. [CrossRef] [PubMed]
86. Chelu, M.; Musuc, A.M.; Popa, M.; Calderon Moreno, J. Aloe Vera-Based Hydrogels for Wound Healing: Properties and Therapeutic Effects. *Gels* **2023**, *9*, 539. [CrossRef]
87. Nakamura-García, A.K.; Santos-Garfias, E.d.C.; Alonso-Martínez, D.I.; Garambullo-Peña, T.I.; Covián-Nares, J.F.; Gómez-Barroso, M.; Montoya-Pérez, R. Healing of Wounds Treated with Chitosan Hydrogels with Extracts from Aloe Vera and Calendula Officinalis. *Rev. Mex. Ing. Bioméd.* **2022**, *43*, 19–31. [CrossRef]

88. Montembault, A.; Viton, C.; Domard, A. Rheometric Study of the Gelation of Chitosan in Aqueous Solution Without Cross-Linking Agent. *Biomacromolecules* **2005**, *6*, 653–662. [CrossRef] [PubMed]
89. Alqaheem, Y.; Alomair, A.A. Microscopy and Spectroscopy Techniques for Characterization of Polymeric Membranes. *Membranes* **2020**, *10*, 33. [CrossRef]
90. Hastings, G. Vibrational Spectroscopy of Photosystem I. *Biochim. Biophys. Acta (BBA)-Bioenerg.* **2015**, *1847*, 55–68. [CrossRef]
91. Freimoser, F.M.; Jakob, C.A.; Aebi, M.; Tuor, U. The MTT [3-(4,5-Dimethylthiazol-2-Yl)-2,5-Diphenyltetrazolium Bromide] Assay Is a Fast and Reliable Method for Colorimetric Determination of Fungal Cell Densities. *Appl. Environ. Microbiol.* **1999**, *65*, 3727–3729. [CrossRef] [PubMed]
92. Torres-Moreno, H.; López-Romero, J.C.; Vázquez-Solorio, J.Y.; Velázquez-Contreras, C.A.; Garibay-Escobar, A.; Díaz-López, R.; Robles-Zepeda, R.E. Antioxidant, Anti-Inflammatory and Antiproliferative Properties of Ibervillea Sonorae. *S. Afr. J. Bot.* **2019**, *125*, 207–213. [CrossRef]
93. Sanapalli, B.K.R.; Yele, V.; Singh, M.K.; Thaggikuppe Krishnamurthy, P.; Karri, V.V.S.R. Preclinical Models of Diabetic Wound Healing: A Critical Review. *Biomed. Pharmacother.* **2021**, *142*, 111946. [CrossRef]
94. Felix, C. *Actividad Antiinflamatoria y Antibacterial de Bursera Linanoe*; Universidad Autónoma del Estado de Morelos: Estado de Morelos, Mexico, 2021.
95. Harold Gomez Actividad Antiinflamatoria de Productos Naturales. *Boletín Latinoam. y del Caribe de Plantas Med. y Aromáticas* **2011**, *10*, 182–217.
96. Olivera-Castillo, L.; Grant, G.; Kantún-Moreno, N.; Acevedo-Fernández, J.J.; Puc-Sosa, M.; Montero, J.; Olvera-Novoa, M.A.; Negrete-León, E.; Santa-Olalla, J.; Ceballos-Zapata, J.; et al. Sea Cucumber (*Isostichopus badionotus*) Body-Wall Preparations Exert Anti-Inflammatory Activity In Vivo. *PharmaNutrition* **2018**, *6*, 74–80. [CrossRef]
97. Salas-Oropeza, J.; Jimenez-Estrada, M.; Perez-Torres, A.; Castell-Rodriguez, A.E.; Becerril-Millan, R.; Rodriguez-Monroy, M.A.; Canales-Martinez, M.M. Wound Healing Activity of the Essential Oil of Bursera Morelensis, in Mice. *Molecules* **2020**, *25*, 1795. [CrossRef] [PubMed]
98. *Estrada-Gerardo Evaluación de la Actividad Antiinflamatoria y Efecto Cicatrizante In Vivo de Extractos Metanólicos de Ibervillea Sonorae*; Universidad de Sonora: Hermosillo, Mexico, 2021.